Master Thesis

HYBRIDISATION OF CONCENTRATED THERMAL SOLAR POWER RECEIVER PLANT WITH GAS TURBINE.

Author: Fernando Noguera Fuentes [1]
Supervisor: José Ignacio Linares Hurtado [2] and Eva Arenas Pinilla[2]

[1] Universidad Pontificia Comillas, Escuela Técnica Superior de Ingeniería – ICAI
[2] Universidad Pontificia Comillas, Escuela Técnica Superior de Ingeniería – ICAI

Abstract: In order to decarbonize the atmosphere and become carbon neutral by 2050, society is constantly pushing for energy generation through renewable resources, such as wind or photovoltaic power plants. However, due to their manageability problems and their difficulty of storage, it is necessary to have grid support technologies that allow energy generation when resources are insufficient or during peak demand hours. Some alternatives identified to solve this problem are solar thermal power plants or CSP (concentrated solar power) because they allow thermal storage through a system of tanks that use molten salts as fluid; or technologies of non-renewable origin, specifically, combined cycle power plants, since they are, of the fossil fuel plants, the ones that emit the least emissions into the atmosphere and the simplest to decarbonize. For all these reasons, the present project proposes the hybridization of a solar tower receiver power plant (CSP) with a combined cycle power plant, thus reducing emissions during hours of high solar radiation thanks to a partial regeneration in the gas turbine, responsible for raising the temperature of the air leaving the compressor before it enters the combustion chamber and, therefore, reducing the need for fuel. In addition, by adding a supercritical CO2 bottoming cycle and an ORC cycle, it will be possible to take advantage of medium and low temperature heat respectively, achieving average efficiencies of 57.2% and a reduction in atmospheric CO2 emissions of up to 32% (under constant cooling and feeding conditions). The plant has been sized to generate 180 MWe and aims to increase the manageability and reduce the investment of CSP plants through the use of combined cycle power plants.

Keywords: combined cycle power plant, central tower receiver, supercritical CO2 cycle, ORC cycle.

1. Introduction

Among the different technologies being developed to provide an uninterrupted energy supply, the use of batteries, molten salt tanks and biofuels, stand out among others. This project proposes the use of a combined cycle power plant hybridised with thermosolar technology, thus allow to reduce natural gas consumption considerably during peak solar hours and allowing for a generation technology that, despite being partially dependent on environmental factors, can also supply electricity on a continuous basis.

2. State of the Art

2.1. Brayton cycles

Brayton cycles are thermodynamic cycles characterized by working with fluids in a gaseous state. However, unlike the Rankine cycle, having to compress a gas increases the consumption of the cycle.

Brayton cycles can be opened, using air as a working fluid (gas cycle) or closed, working in this case with fluids that provide greater efficiency (supercritical CO_2 cycle or helium cycle). An advantage of the closed cycle is that it allows, unlike an open one, that the minimum working pressure is above the atmospheric one, which reduces the specific volume of the fluid, consequently decreasing the consumption of the compressor.

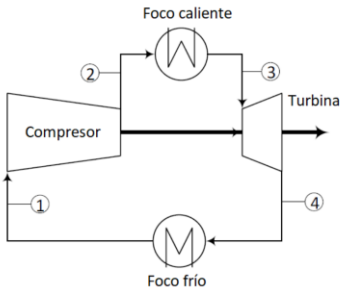

Figure 1: Single Brayton cycle closed.

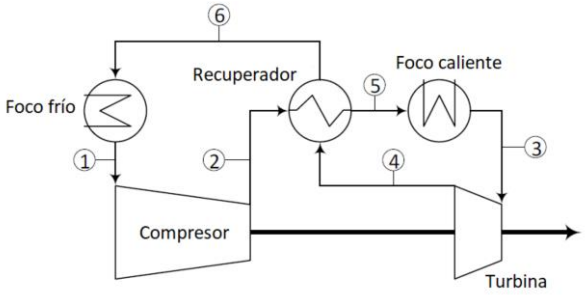

Figure 2: Brayton cycle closed with intermediate heat recovery.

2.2. Recompression cycles

Within the cycles that use supercritical CO_2 as a working fluid, the recompression cycle must be highlighted. This is because, when S-CO_2 is used, the higher the cycle pressure, the higher the specific heat, which causes an imbalance in the heat recuperator of a closed Brayton cycle (Figure 2). The solution to this problem is the division of the heat recuperator into two units, a heat recuperator that works at low temperatures (LTR) and another that works at high temperatures (HTR).

The most remarkable feature of the recompression cycle is that the low temperature recuperator has two different mass flows due to the addition of a degree of freedom (α). Figure 3 shows how, in point 4, there is a division of the mass flow into two currents, a first directed to an auxiliary compressor, which returns the fluid at high pressure to the HTR; and a second division that directs the S-CO_2 towards the main compressor, which compresses the fluid in conditions close to its critical point (due to the previous passage through the cold focus). After being compressed, the fluid leaving the main compressor at high pressure is directed back towards the LTR and joined with the previously diverted fluid. The current 3-4 (low pressure and low specific heat) crosses the LTR with a mass flow greater than the current 6-7, at higher pressure and with greater specific heat. By adjusting the fraction of flow (α) that passes through the auxiliary compressor, it can be achieved that the heat capacity of both currents is similar, which allows to have a T-Q profile balanced, which reduces the destruction of exergy inside, considerably reducing losses.

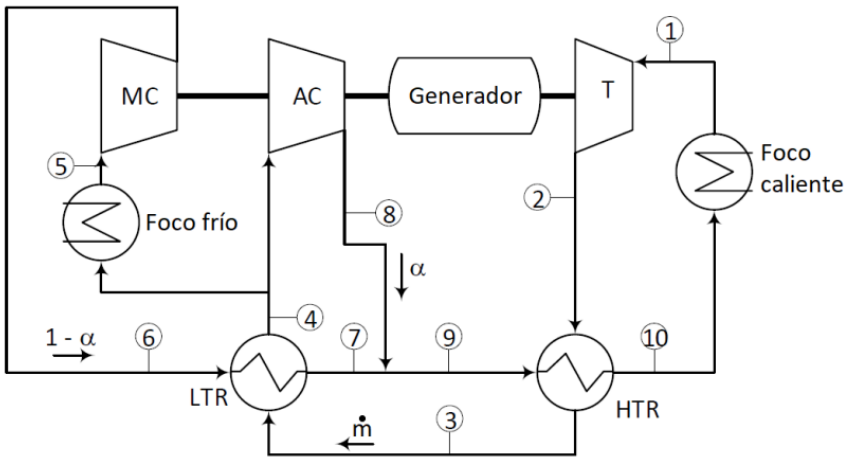

Figure 3: Recompression cycle.

The recompression cycle fed at low pressure differs from the conventional one in that the hot focus is no longer located at the entrance of the turbine, but at its exit, giving greater relevance to the HTR heat exchanger, which becomes the bridge between the thermal source and the fluid upstream of the turbine. This modification gives several advantages to the cycle (such as the increase of the pressure of the cycle or the reduction of size of the heat exchangers) at the cost of needing to slightly increase the temperature at the exit of the hot spot, which translates into a slight increase in fuel.

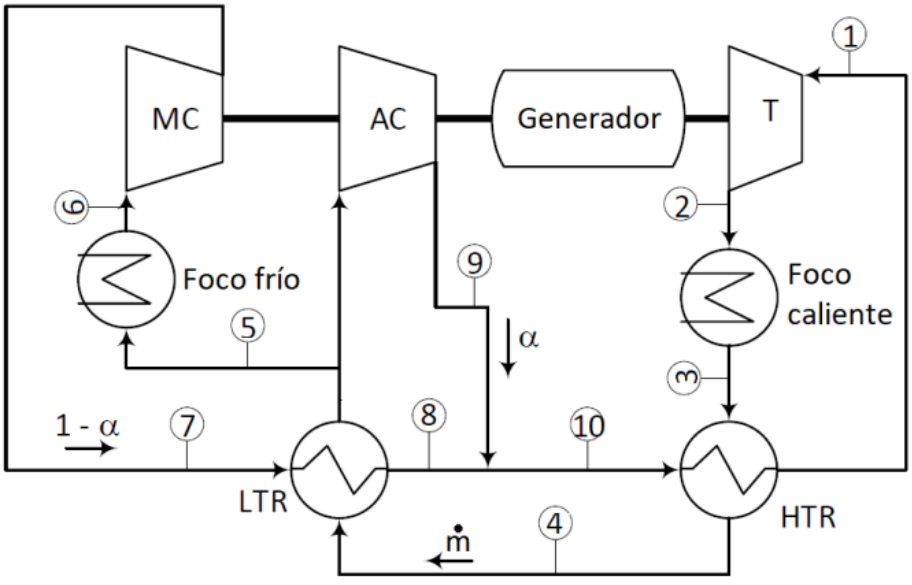

Figure 4: Recompression cycle fed at low pressure.

3. Objectives

The hybridisation of a combined cycle power plant with a solar thermal power plant addressed in this project consists of using a regenerative gas turbine as the topping cycle and a supercritical CO_2 cycle as the bottoming cycle. The S-CO_2 power cycle receives heat from two thermal sources: one high temperature and one intermediate temperature. The high-temperature thermal source is a

parallel between the turbine outlet of the topping cycle (High Temperature Heat Recovery, HTHR) and the solar receiver (Central Tower Receiver, CTR). The Intermediate Temperature Heat Recovery (ITHR) uses the exhaust gases from the gas turbine. These are obtained after mixing the gases coming from the gas turbine recuperator, together with those coming from the HTHR (gas turbine outlet). The waste heat available downstream of the ITHR heat exchanger is collected in another heat recovery unit, a low temperature heat recovery unit (LTHR) and converted into electricity by means of an Organic Rankine Cycle (ORC). In the S-CO_2 power cycle the heat rejection is carried out by a cooling tower through the Precooler (PC), whereas, in the ORC, it is carried out through the condenser (COND).

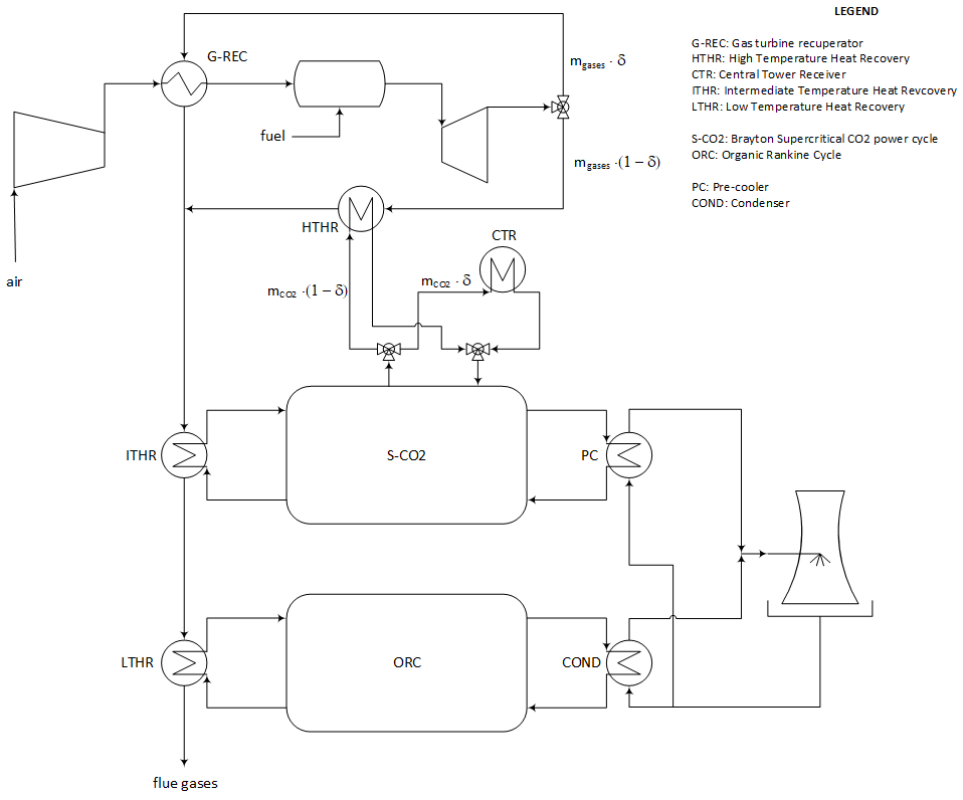

Figure 5: Conceptual scheme of the proposed plant.

4. Methodology

After brief description of the elements that make up the hybridization of the combined cycle with the solar thermal power plant, the methodology used in the modeling will be described.

4.1. Cycle analysis

The fact of maintaining a continuous supply of energy to the grid to supply the needs of society, together with the need to decarbonize the atmosphere for Horizon 2050, has led to the implementation of new methods of energy generation that, until a few years ago, were not considered. The idea developed on this project is the hybridization of a combined cycle power plant with a solar thermal receiver, using as a secondary cycle to maximize efficiency a supercritical CO_2 cycle and implementing an ORC cycle aimed at taking advantage of the waste heat of the exhaust gases of the plant.

Figure 5 shows the conceptual diagram of the plant in which a gas cycle is used as the topping cycle and a S-CO_2 cycle is used as the bottoming one. There is also an ORC cycle intended to take advantage of the remaining waste heat after the exchange of medium temperature with the S-CO_2 cycle. Instead, Figure 6 shows a more detailed view of the plant, in which all the elements that compose the combined cycle can be observed.

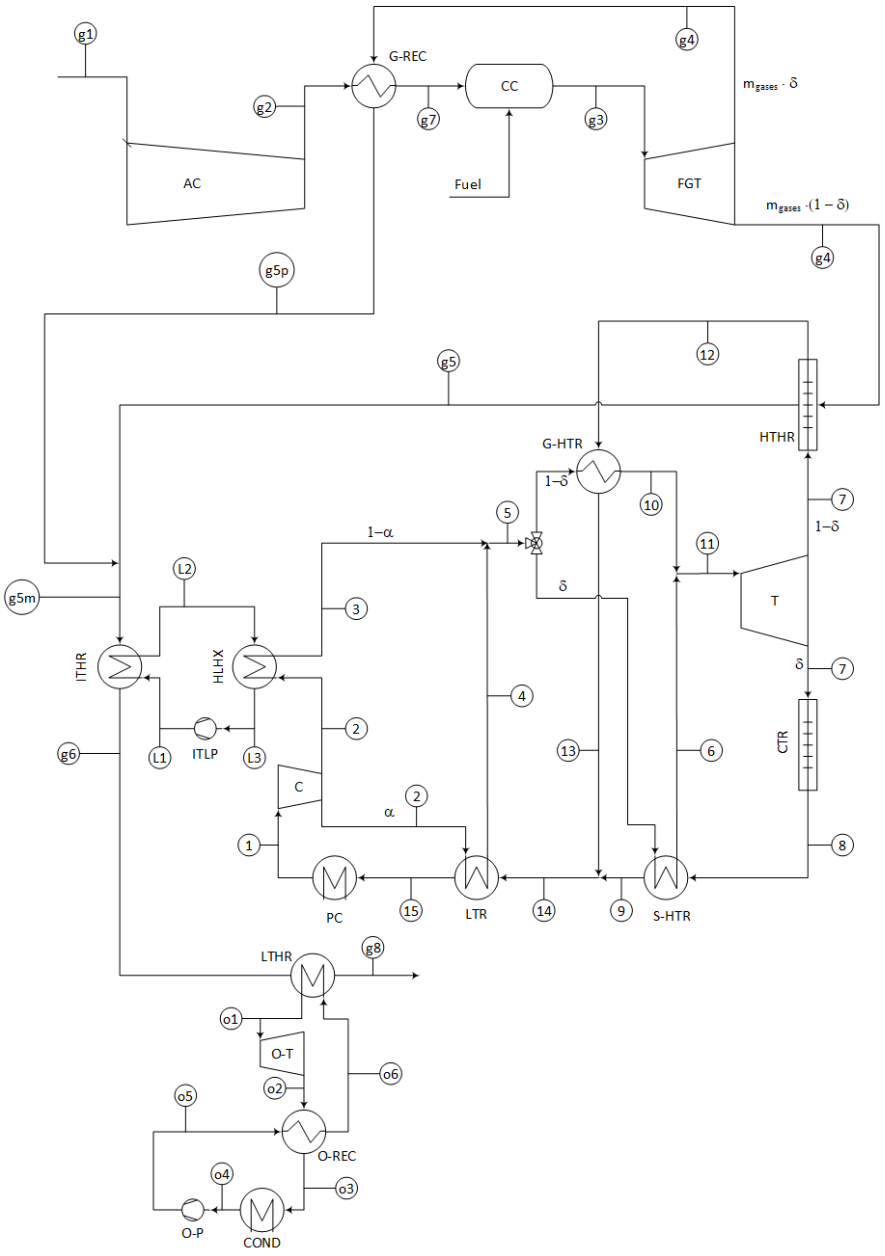

Figure 6: Hybridization of combined cycle with solar thermal power plant.

4.1.1. Gas cycle

The gas cycle is an open Brayton Cycle, which is constituted with the main elements of it:

- Compressor: increases the inlet pressure of the air from the atmospheric (1 bar) to about 6 bar.

- Combustion chamber: place where the oxidizer is inflamed, making the contribution of thermal energy to the fluid and increasing its temperature from 257 °C obtained after compression to 1500 °C.
- Turbine: responsible for transforming the thermal energy of the fluid into electrical energy, reducing the pressure of the fluid from the 6 bar previously mentioned to the atmospheric pressure. The combustioned air leaves the turbine at a temperature close to 940 °C, so it is necessary to use the bottoming cycle of supercritical CO_2 to take advantage of this waste heat.

However, as can be seen in Figure 7, this cycle has some additional elements responsible for reducing fuel consumption in the hours of maximum solar radiation. The first element that is appreciated is the gas turbine recuperator (g2-g7), which is a cross-flow heat exchanger (plates with fins). In second instance, it is observed that the turbine has two different output channels, one directly directed towards the S-CO_2 cycle (g4-g5), while the other is directed towards the gas turbine recuperator (g4-g5p), rejoining both flows at the entrance of the loop cycle (g5m).

As will be seen later, the S-CO_2 cycle receives high-temperature heat from two sources in parallel: the exhaust gases from the gas turbine and the solar receiver, so during the central hours of the day it is not necessary to provide heat in the high temperature exchanger or HTHR (cross-flow exchanger); in those central hours all the exhaust gases that leave the turbine will be directed towards the heat recuperator (direction g4-g5p), increasing the temperature of the fluid prior to its entry into the combustion chamber from 257 °C to approximately 705 °C, which considerably reduces the amount of fuel needed to reach the 1500 °C needed at the inlet of the gas turbine. As solar radiation decreases, the amount of flow diverted to the gas turbine recuperator (γ) will be reduced, increasing the mass flow that will be directed towards the HTHR exchanger. To compensate for the heat not provided in the regenerator, more fuel will be provided in the combustion chamber. At the moment when solar radiation is non-existent, fluid will stop passing through the heat recuperator (g4-g5p) and all the flow will go to the HTHR exchanger.

After the separation of both flows at the outlet of the gas turbine, these will be mixed back to the inlet of the medium temperature exchanger (ITHR), a cross-flow heat exchanger (tubes with fins), at 540 °C and the fluid will continue on its way to the heat exchanger with the ORC cycle with an inlet temperature of approximately 335 °C. Finally, the exhaust gases will be expelled at atmospheric pressure and at a temperature above 100 °C, avoiding the condensation of H_2O droplets mixed with other compounds such as NO_x or S_2O, which are capable of corroding the chimney pipes.

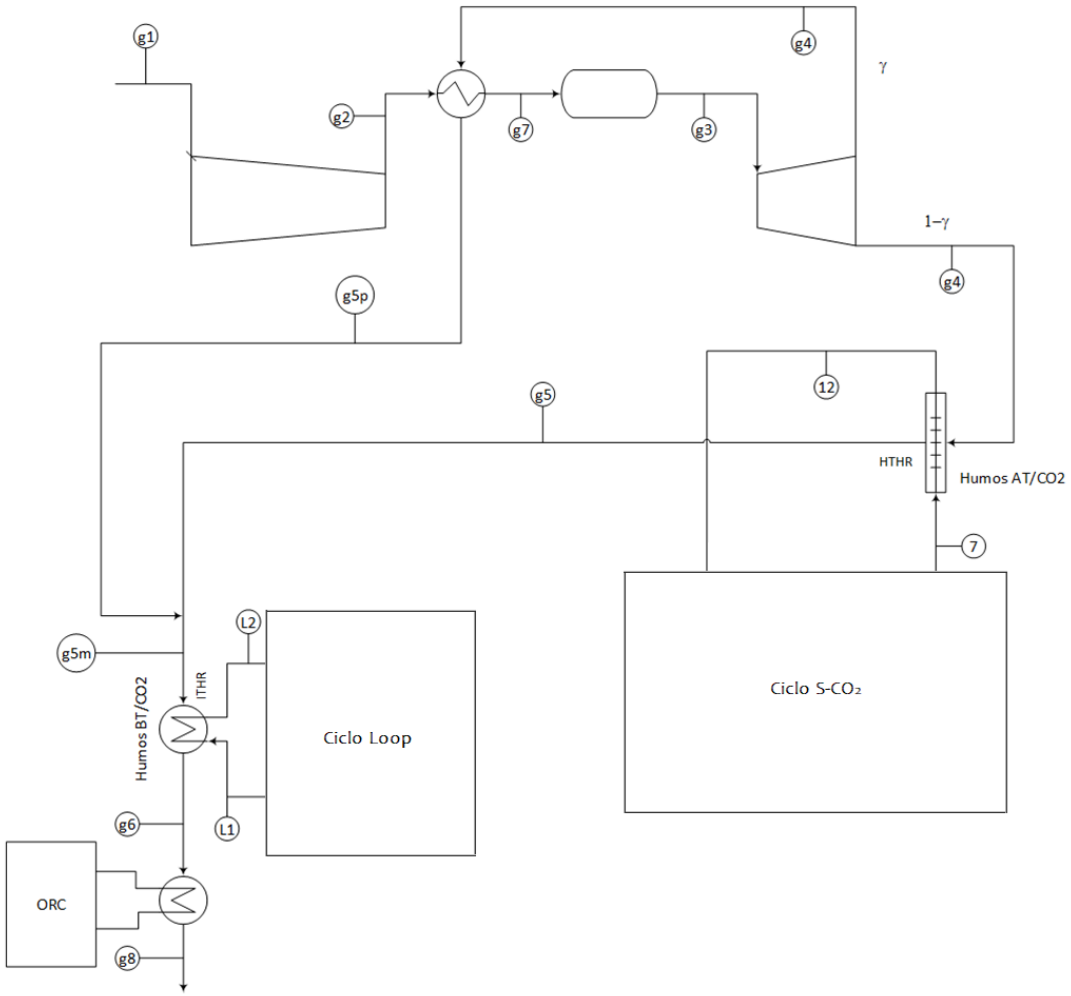

Figure 7: Gas cycle.

In order to perform the modeling of the gas cycle, it has been necessary to assume a series of internal conditions of the cycle.

- The air will enter at the compressor at a temperature of 15 °C and at a pressure of 1 bar. It will be expelled from the cycle at atmospheric pressure.
- The temperature of the fluid after passing through the combustion chamber shall be 1500 °C. In addition, it is assumed that complete combustion is carried out and that the fuel is pure methane, which enters the combustion chamber at 25 °C.
- The efficiency of the compressor will be estimated at 85%, while that of the turbine efficiency will be 90%.
- The exhaust gases of the gas cycle must have a temperature higher than 100 °C to avoid problems related to corrosion and wear of the pipes.
- The turbine outlet temperature is set at 950 °C and produces a network of 100 MWe.

4.1.2. S-CO_2 cycle

The S-CO_2 cycle receives heat at two temperature levels (Figure 6**¡Error! No se encuentra el origen de la referencia.**). High-temperature reception can proceed in parallel from the exhaust gases at the turbine outlet (HTHR) or solar receiver (CTR), while low-temperature reception comes from mixing the low-pressure outlet of the turbine regenerator with that of the HTHR recuperator via the ITHR. Since the latter is a cross-flow heat exchanger (tubes and fins) an intermediate loop of CO_2 is used, so that heat is transferred from the IHTR to a loop at 85 bar, and from there by a PCHE to the main circuit (approximately at 300 bar).

Once the reception of heat at high temperature has occurred, the heat transfer to the high-pressure current that is directed towards the turbine is carried out by means of the HTR heat exchangers (PCHE), both heat exchangers receive the heat from their respective thermal source and rejoin their flows after the exchange, meeting the LTR heat exchanger (PCHE), which provides medium temperature heat to a fraction (α) of the medium pressure flow. After passing through the LTR, the fluid is directed towards the Precooler or PC (PCHE) where it reduces its temperature to 35 °C, remaining close to the critical point, which considerably increases the density of CO_2 and decreases the work exerted by the compressor.

Finally, after the contribution of medium temperature heat, from both, LTR and auxiliary loop, the fluid is directed back towards the HTR exchangers, receiving the high temperature heat to enter into the turbine.

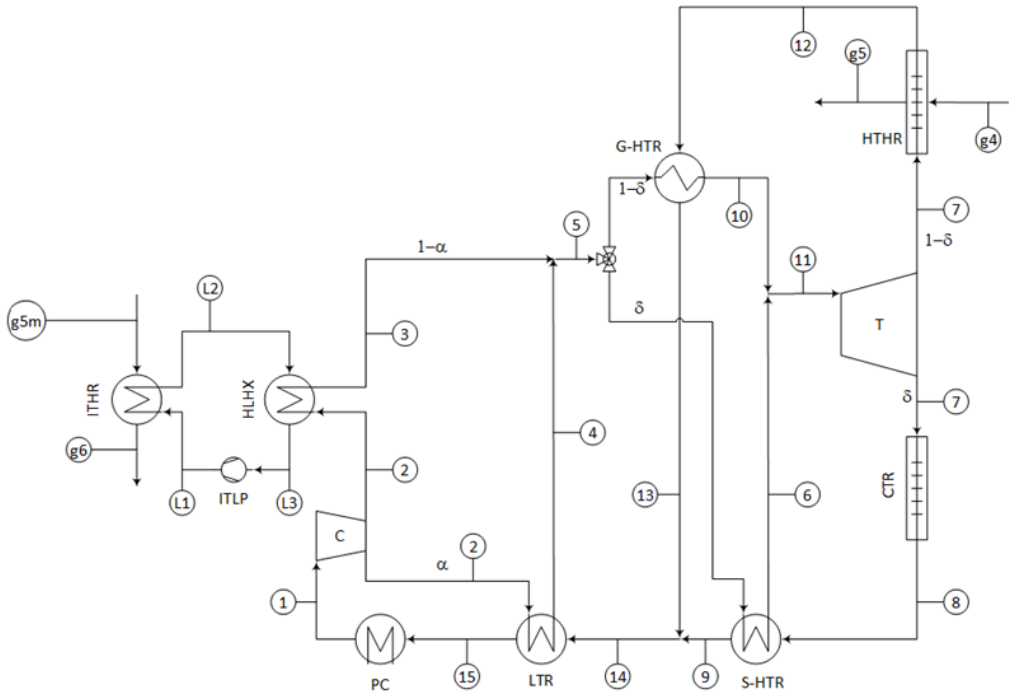

Figure 8: Loop cycle and S-CO_2 cycle.

The operating conditions established for the resolution of this cycle are as follows:

- Temperature of S-CO_2 prior to its passage through the respective HTR exchangers will be 700 °C.

- Pitch point of the HTR interchange will be 15 °C, that of the LTR will be 5 °C and that of the HTHR will be 30 °C.
- Turbine efficiency will be estimated at 92%, while that of the compressor will be 87%.
- Pressure drops in exchangers using S-CO_2 as a fluid is 40 kPa.
- Pressure in the high zone will be about 300 bar, while in the low zone it will be around 85 bar.
- Coefficients of delta (δ), beta (β) and gamma (γ) will be exactly the same at all times.
- The efficiency of the pump belonging to the loop cycle will be 75% and the heat exchanger with the S-CO_2 cycle will have a Pitch Point of 5 °C.
- Pressure of the Loop Cycle will be 85 bar.

4.1.3. ORC Cycle

As Figure 9 shows, the ORC cycle used is an Organic Rankine Cycle that has an intermediate heat recuperator.

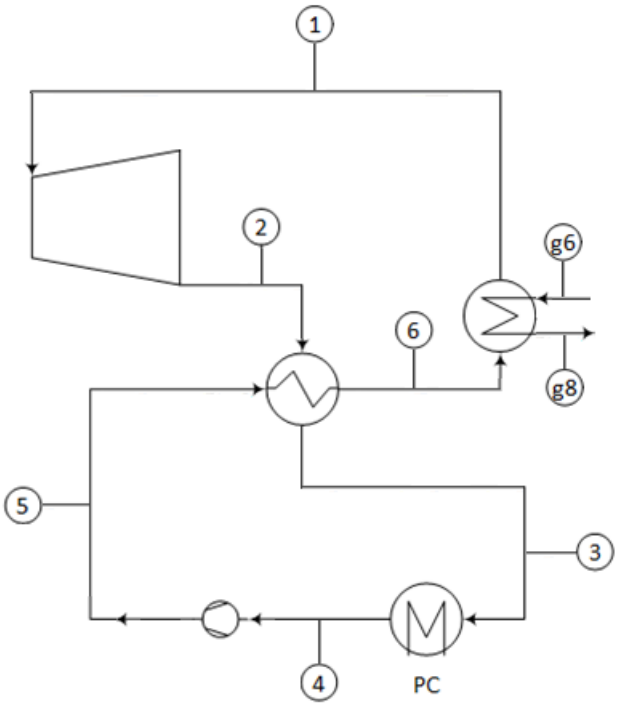

Figure 9: ORC Cycle.

Its established operating conditions are:

- The estimated turbine efficiency is 80%, while the pump is 75%.
- The temperature of the fluid after condensation (4) will be 35 °C and, in addition, as the next element of the cycle is a pump, the fluid will be in liquid state to avoid cavitation.
- The pressure on the high-pressure side of the ORC cycle will be 50 bar and an inlet temperature to the turbine will be close to 200 °C.
- The Pitch Point of the heat recuperator is 10 °C.

4.1.4. Cooling circuit

The cooling circuit consists of 3 clearly differentiated elements.

- Cooling tower: equipment responsible for cooling the water through the principle of evaporative cooling, in which the hot water is sprayed in the form of droplets to cool itself from a stream of air flowing in the opposite direction. The chilled water is collected and redistributed through the cooling circuit. A contribution is required to replace the evaporated water.
- Pump: responsible for overcoming pressure losses.
- Exchanger: allows water to absorb heat from the fluid circulating through the power circuit.

Due to the fact that two cooling circuits are necessary throughout the plant, it has been decided to size two different cooling circuits, a first that is responsible for cooling the S-CO_2 (PC) and a second one in charge of condensing the R-600 (C ORC).

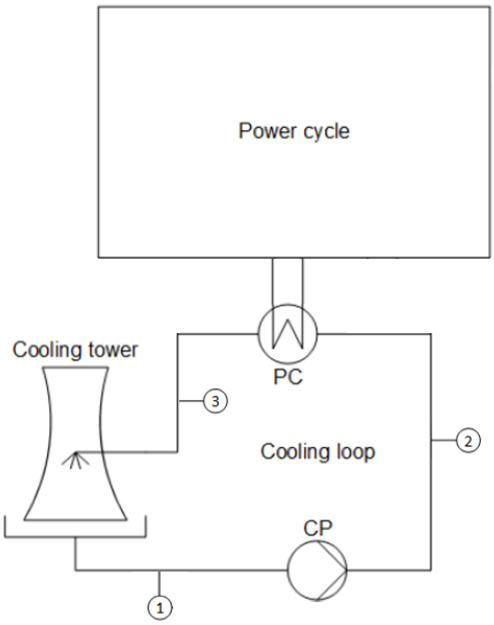

Figure 10: Cooling circuit.

To size the cooling circuits, it has been established that:

- Water will enter the cooling tower at 30 °C and 5 bar and leave it at atmospheric pressure and 25 °C.
- Water pressure at the pump outlet will be 6 bar.

4.1.5. Cycle calculations

To perform the model calculations in the EES program, all turbomachines have been assumed to be adiabatic. The working pressures of the plant have been chosen to maximize its efficiency.

The abbreviations used during formulation are:

- $\dot{m}$: mass flow.
- $\dot{n}_f$: flow of fuel used.
- Q: heat exchange.

- h: enthalpy.
- s: entropy.
- T: temperature.
- p: pressure.
- Δp: pressure variation.
- ε: effectiveness of the exchanger.
- NTU: number of units transferred.
- UA: variable used for the analysis and design of heat exchangers.
- α, β, γ, δ: internal variables of the model that reflect the amount of solar radiation absorbed by the receiver.
- λ: excess air in the mixture.
- η: performance.
- Ẇ: work.
- Cp: critical power.

Subscripts:

- i: inlet. Used to refer to the entry points of components.
- or: outlet. Used to refer to the exit points of components.
- A: high pressure zone of the exchangers.
- B: low pressure zone of the exchangers.
- PP: pitch point.
- T: turbine.
- C: compressor.
- CComb: combustion chamber.
- REG: regenerative.
- REC: heat recovery.
- CTR: Solar receiver.

4.1.5.1. Common equations.

Turbines:

$$\eta_T = \frac{h_i - h_o}{h_i - h_{os}} \quad (1)$$

$$h_{os} = h(s_i; p_o) \quad (2)$$

$$\dot{W}_T = \dot{m}_T \cdot (h_i - h_o) \quad (3)$$

Compressor:

$$\eta_C = \frac{h_{os} - h_i}{h_o - h_i} \quad (4)$$

$$h_{os} = h(s_i; p_o) \quad (5)$$

$$\dot{W}_C = \dot{m}_C \cdot (h_o - h_i) \quad (6)$$

Pipe joints:

$$p_1 = p_2 \quad (7)$$

$$(1-\beta)\cdot h_1 + \beta \cdot h_2 = h_3 \quad (8)$$

Total power:

$$\dot{W}_{CC} = \dot{W}_{GAS} + \dot{W}_{S-CO2} + \dot{W}_{ORC} \quad (9)$$

$$\eta_{CC} = \frac{\dot{W}_{GAS} + \dot{W}_{S-CO2} + \dot{W}_{ORC}}{Q_{CC} + Q_{REC}} \quad (10)$$

Emissions:

$$G_e = \frac{\dot{n}_f \cdot 16 \cdot 1000 \cdot 3600}{\dot{W}_{GAS} + \dot{W}_{S-CO2} + \dot{W}_{ORC}} \quad (11)$$

$$emissions_{CO2} = G_e \cdot \frac{44}{16} \quad (12)$$

4.1.5.2. Gas Cycle

$$Cp_{GAS} = \frac{\left(\dot{n}_f \cdot \left(\bar{h}_{GAS}(T_{GAS-ORCi};\lambda) - \bar{h}_{GAS}(T_{GAS-ORCo};\lambda)\right)\right)}{\left(\dot{m}_{Aire} + 16 \cdot \dot{n}_f\right)\cdot (T_{GAS-ORCi} - T_{GAS-ORCo})} \quad (13)$$

$$\bar{h}_{COMB} = \bar{h}_{fCO2} + 2\cdot \bar{h}_{fH2O} - \bar{h}_{fCH4} \quad (14)$$

$$\dot{W}_{GAS} = \dot{W}_T - \dot{W}_C \quad (15)$$

$$\dot{m}_{Aire} = \dot{n}_f \cdot 2 \cdot (1+\lambda)\cdot (32 + 3{,}76 \cdot 28) \quad (16)$$

$$\dot{m}_{GAS} = \dot{m}_{Aire} + \dot{n}_f \cdot 16 \quad (17)$$

Combustion chamber:

$$\begin{aligned} &44\cdot h(CO2;T=T[CCombo]) + 2\cdot h(H2O;T=T[CCombo])\cdot 18 + 7{,}52\cdot(1+\lambda)\cdot h(N2;T=T[CCombo]) \\ &\quad \cdot 28 + 2\cdot\lambda\cdot h(O2;T=T[CCombo])\cdot 32 \\ &\quad = 2\cdot(1+\lambda)\cdot h(O2;T=T[CCombi])\cdot 32 + 7{,}52\cdot(1+\lambda)\cdot h(N2;T=T[CCombi])\cdot 28 \\ &\quad + h(CH4;T=25)\cdot 16 \end{aligned} \quad (18)$$

$$Q_{CComb} = \dot{n}_f \cdot \left|\bar{h}_{COMB}\right| \quad (19)$$

Air compressor:

$$\begin{aligned} &s(O2;T=T_{Ci};p=p_{Ci})\cdot 32 + 3{,}76\cdot s(N2;T=T_{Ci};p=p_{Ci})\cdot 28 \\ &\quad = s(O2;T=T_{sCo};p=p_{Co})\cdot 32 + 3{,}76\cdot s(N2;T=T_{sCo};p=p_{Co})\cdot 28 \end{aligned} \quad (20)$$

$$\begin{aligned} &\eta_C\cdot(h(O2;T=T_{Co})\cdot 32 + 3{,}76\cdot h(N2;T=T_{Co})\cdot 28 - h(O2;T=T_{Ci})\cdot 32 - 3{,}76\cdot h(N2;T=T_{Ci})\cdot 28) \\ &\quad = (h(O2;T=T_{Cso})\cdot 32 + 3{,}76\cdot h(N2;T=T_{Cso})\cdot 28 - h(O2;T=T_{Ci})\cdot 32 - 3{,}76 \\ &\quad \cdot h(N2;T=T_{Ci})\cdot 28) \end{aligned} \quad (21)$$

$$\begin{aligned} \dot{W}_C = \dot{n}_f \cdot 2\cdot(1+\lambda)\cdot h(O2;T=T_{Co})\cdot 32 + 3{,}76\cdot h(N2;T=T_{Co})\cdot 28 - h(O2;T=T_{Ci})\cdot 32 - 3{,}76 \\ \cdot h(N2;T=T_{Ci})\cdot 28 \end{aligned} \quad (22)$$

Gas turbine:

$$\bar{s}(p_{Ti}; T_{Ti}; \lambda) = \bar{s}(p_{To}; T_{Tso}; \lambda) \quad (23)$$

$$\eta_T = \frac{\bar{h}(T_{Ti}; \lambda) - \bar{h}(T_{To}; \lambda)}{\bar{h}(T_{Ti}; \lambda) - \bar{h}(T_{Tso}; \lambda)} \quad (24)$$

$$\dot{W}_T = \dot{n}_f \cdot (\bar{h}(T_{Ti}; \lambda) - \bar{h}(T_{To}; \lambda)) \quad (25)$$

Gas cycle regenerator: 258

$$\gamma \cdot (\overline{h}(T_{Bi}; \lambda) - \bar{h}(T_{Bo}; \lambda)) = 2 \cdot (1 + \lambda) \cdot (h(O2; T = T_{Ao}) \cdot 32 + 3{,}76 \cdot h(N2; T = T_{Ao}) \cdot 28 - h(O2; T = T_{Ai}) \cdot 32 - 3{,}76 \cdot h(N2; T = T_{Ai}) \cdot 28) \quad (26)$$

$$Q_{REG} = \dot{n}_f \cdot 2 \cdot (1 + \lambda) \cdot (h(O2; T = T_{Ao}) \cdot 32 + 3{,}76 \cdot h(N2; T = T_{Ao}) \cdot 28 - h(O2; T = T_{Ai}) \cdot 32 - 3{,}76 \cdot h(N2; T = T_{Ai}) \cdot 28) \quad (27)$$

$$\dot{m}_{AN} = \dot{n}_{fN} \cdot 2 \cdot (1 + \lambda_N) \quad (28)$$

$$\dot{m}_{BN} = \dot{n}_{fN} \quad (29)$$

$$\dot{m}_A = \dot{n}_f \cdot 2 \cdot (1 + \lambda) \quad (30)$$

$$\dot{m}_B = \dot{n}_f \cdot \gamma \quad (31)$$

$$UA \cdot \frac{(\dot{m}_A^{0,8} + \dot{m}_B^{0,8})}{UA_N} = \dot{m}_A^{0,8} \cdot \dot{m}_B^{0,8} \cdot \frac{(\dot{m}_A^{0,8} + \dot{m}_B^{0,8})}{\dot{m}_{AN}^{0,8} \cdot \dot{m}_{BN}^{0,8}} \quad (32)$$

$$mCp_A = \gamma \cdot \dot{n}_f \cdot 2 \cdot (1 + \lambda) \cdot (h(O2; T = T_{Ao}) \cdot 32 + 3{,}76 \cdot h(N2; T = T_{Ao}) \cdot 28 - h(O2; T = T_{Ai}) \cdot 32 - 3{,}76 \cdot h(N2; T = T_{Ai}) \cdot 28)/(T_{Ao} - T_{Ai}) \quad (33)$$

$$mCp_B \cdot (T_{Bi} - T_{Bo}) = \dot{n}_f \cdot \gamma \cdot (\overline{h}(T_{Bi}; \lambda) - \bar{h}(T_{Bo}; \lambda)) \quad (34)$$

$$mCp = \min(mCp_A; mCp_B) \quad (35)$$

$$NTU \cdot mCp = UA \quad (36)$$

$$\varepsilon = h_x('counterflow'; NTU; mCp_A; mCp_B; "\varepsilon") \quad (37)$$

$$\varepsilon \cdot mCp \cdot (T_{Bi} - T_{Ai}) = Q_{REG} \quad (38)$$

4.1.5.3. S-CO_2 cycle 259

HTHR: 260

$$Q_{HTHR} = \dot{n}_f \cdot \left(\bar{h}(T_{GASi}; \lambda) - \bar{h}(T_{GASo}; \lambda)\right) \quad (39)$$

$$Q_{HTHR} = \dot{m} \cdot (1 - \delta) \cdot (h_i - h_o) \quad (40)$$

$$\varepsilon_{HTHR} = \frac{T_{GASi} - T_{GASo}}{T_{GASi} - T_i} \quad (41)$$

$$mCp_{CO2} = \dot{m} \cdot (1 - \delta) \cdot \left(\frac{h_o - h_i}{T_o - T_i}\right) \quad (42)$$

$$mCp_{GAS} = \dot{m}_f \cdot \left(\frac{\left(\bar{h}(T_{GASi}; \lambda) - \bar{h}(T_{GASo}; \lambda) \right)}{T_{GASi} - T_{GASo}} \right) \quad (43)$$

$$NTU_{CRAT} = h_x('crossflow\ both\ unmixed'; \varepsilon_{HTHR}; mCp_{GAS}; mCp_{CO2}; "NTU") \quad (44)$$

$$NTU_{HTHR} = \frac{UA_{HTHR}}{mCp_{GAS}} \quad (45)$$

$$T_{GASo} = T_i + PP_{HTHR} \quad (46)$$

$$p_o = p_i - \Delta p_{CO2} \quad (47)$$

HTR & LTR:

$$PP_{HTR} = T_{Bo} - T_{Ai} \quad (48)$$

$$\dot{m}_B \cdot (h_{Bi} - h_{Bo}) = \dot{m}_A \cdot (h_{Ao} - h_{Ai}) \quad (49)$$

$$Q_{HTR} = \dot{m}_B \cdot (h_{Bi} - h_{Bo}) \quad (50)$$

$$p_{Bo} = p_{Bi} - \Delta p_{CO2} \quad (51)$$

$$p_{Ao} = p_{Ai} - \Delta p_{CO2} \quad (52)$$

$$\varepsilon_{HTR} = \frac{T_{Bi} - T_{Bo}}{T_{Bi} - T_{Ai}} \quad (53)$$

$$NTU_{HTR} = \frac{\varepsilon_{HTR}}{(1 - \varepsilon_{HTR})} \quad (54)$$

$$NTU_{HTR} = \frac{UA_{HTR}}{mCp_{Bi-Bo}} \quad (55)$$

$$mCp_{Bi-Bo} = \dot{m}_B \cdot \left(\frac{h_{Bi} - h_{Bo}}{T_{Bi} - T_{Bo}} \right) \quad (56)$$

Solar Receiver:

$$Q_{CTR} = \dot{m} \cdot \delta \cdot (h_i - h_o) \quad (57)$$

$$p_o = p_i - \Delta p_{CO2} \quad (58)$$

Loop Cycle Exchanger:

$$\dot{m}_{CO2} \cdot (h_{CO2o} - h_{CO2i}) = \dot{m}_{Loop} \cdot (h_{Li} - h_{Lo}) \quad (59)$$

$$p_{CO2o} = p_{CO2i} - \Delta p_{CO2} \quad (60)$$

$$T_{Lo} = T_i + PP_{Loop} \quad (61)$$

$$p_{Lo} = p_{Li} - \Delta p_{CO2} \quad (62)$$

$$T_{Li} = T_{CO2o} + PP_{Loop} \quad (63)$$

$$Q_{CO2} = \dot{m}_{CO2} \cdot (h_{CO2o} - h_{CO2i}) \quad (64)$$

Loop Cycle Pump: 264

$$\eta_{Pump} = \frac{h_{Lo} - h_{Li}}{h_{Lso} - h_{Li}} \quad (65)$$

$$\dot{W}_{Pump} = \dot{m}_L \cdot (h_{Lo} - h_{Li}) \quad (66)$$

ITHR: 265

$$Q_{IHTR} = \dot{n}_f \cdot \left(\bar{h}(T_{GASi}; \lambda) - \bar{h}(T_{GASo}; \lambda)\right) \quad (67)$$

$$Q_{IHTR} = \dot{m}_L \cdot (h_{Li} - h_{Lo}) \quad (68)$$

$$p_{Lo} = p_{Li} - \Delta p_{CO2} \quad (69)$$

PC: 266

$$Q_{PC} = \dot{m} \cdot (h_i - h_o) \quad (70)$$

$$p_o = p_i - \Delta p_{CO2} \quad (71)$$

Power and performance cycle S-CO2: 267

$$\dot{W}_{S-CO2} = \dot{W}_T - \dot{W}_C - \dot{W}_{Pump} \quad (72)$$

$$\eta_{S-CO2} = \frac{\dot{W}_{S-CO2}}{Q_{HTHR} + Q_{CTR} + Q_{ITHR}} \quad (73)$$

4.1.5.4. ORC Cycle 268

$$\dot{m}_{GAS} = \dot{m}_{AIRE} + 16 \cdot \dot{n}_f \quad (74)$$

$$\dot{m}_{GASN} = \dot{m}_{AIREN} + 16 \cdot \dot{n}_{fN} \quad (75)$$

$$Q_{INT\ GAS} = \dot{m}_{GAS} \cdot Cp_{GAS} \cdot (T_{GASi} - T_{GASo}) \quad (76)$$

$$\dot{m} = \dot{m}_N \quad (77)$$

$$Cp_{GAS} = 1{,}109 \quad (78)$$

$$mCp_{GAS} = \dot{m}_{GAS} \cdot Cp_{GAS} \quad (79)$$

$$mCp_{GAS} = mCp \quad (80)$$

$$\eta_{ORC} = \frac{w_T - w_{Pump}}{q_{CAL}} \quad (81)$$

$$\dot{W}_{ORC} = \dot{W}_T - \dot{W}_{Pump} \quad (82)$$

Turbine: 269

$$p_i - p_o = (p_{Ni} - p_{No}) \cdot \left(\frac{\dot{m}}{\dot{m}_N}\right)^2 \quad (83)$$

Regenerator: 270

$$h_{Bi} - h_{Bo} = h_{Ao} - h_{Ai} \quad (84)$$

$$Q_{REG} = \dot{m} \cdot q_{REG} \quad (85)$$

$$T_{Bo} = T_{Ai} + PP_{REG} \quad (86)$$

$$p_{Bi} = p_{Bo} \quad (87)$$

$$p_{Ai} = p_{Ao} \quad (88)$$

$$q_{REG} = h_{Bi} - h_{Bo} \quad (89)$$

$$\varepsilon_{REG} \cdot mC_B \cdot (T_{Bi} - T_{Ai}) = Q_{REG} \quad (90)$$

$$mC_B = \dot{m} \cdot Cp_B \quad (91)$$

$$Cp_B = 2{,}012 \quad (92)$$

$$mC_A = \dot{m} \cdot Cp_A \quad (93)$$

$$Cp_A = 2{,}677 \quad (94)$$

$$NTU_{REG} = h_x('counterflow'; \varepsilon_{REG}; mC_B; mC_A; "NTU") \quad (95)$$

$$NTU_{REG} = \frac{UA_{REG}}{mC_B} \quad (96)$$

$$\frac{UA_{REG}}{UA_{REGN}} = \left(\frac{\dot{m}}{\dot{m}_N}\right)^{0,8} \quad (97)$$

PC ORC: 271

$$p_i = p_o \quad (98)$$

$$q_{CON} = h_i - h_o \quad (99)$$

$$Q_{CON} = \dot{m} \cdot q_{CON} \quad (100)$$

Pump: 272

$$\eta_{Pump} \cdot (h_o - h_i) = v_i \cdot (p_o - p_i) \cdot 100 \quad (101)$$

$$w_{Pump} = (h_o - h_i) \quad (102)$$

$$\dot{W}_{Pump} = \dot{m} \cdot w_{pump} \quad (103)$$

Gas Cycle Exchanger: 273

$$q_{CAL} = h_o - h_i \quad (104)$$

$$Q_{CAL} = \dot{m} \cdot q_{CAL} \quad (105)$$

$$p_i = p_o \quad (106)$$

$$UA_{CAL} \cdot \frac{\left(\dot{m}^{0,8} + \dot{m}_{GAS}^{0,8}\right)}{UA_{CALN}} = \dot{m}^{0,8} \cdot \dot{m}_{GAS}^{0,8} \cdot \left(\frac{\dot{m}_N^{0,8} + \dot{m}_{GASN}^{0,8}}{\dot{m}_N^{0,8} \cdot \dot{m}_{GASN}^{0,8}}\right) \quad (107)$$

$$mC_{ORC} \cdot (T_o - T_i) = \dot{m} \cdot (h_o - h_i) \quad (108)$$

$$NTU_{CAL} = \frac{UA_{CAL}}{mCp} \quad (109)$$

$$\varepsilon_{CAL} = h_x('crossflow\ both\ unmixed'; NTU_{CAL}; mCp_{GAS}; mC_{ORC}; "\varepsilon") \quad (110)$$

$$Q_{GAS} = \varepsilon_{CAL} \cdot mCp \cdot (T_{GASi} - T_i) \quad (111)$$

4.2. Properties of fluids

Air and exhaust gases have been modeled as ideal gases, while CO_2 and R-600 as pure substances. These models are collected in the "Engineering Ecuation Solver" or "EES" environment.

4.2.1. Air and exhaust gases

The properties of air as an ideal gas are implemented in EES through the correlations of Lemmon et al. [1], valid between 100 °K and 2000 °K. In the case of exhaust gases, the properties of the mixture have been calculated assuming a complete combustion with methane, whose excess air has been determined according to the desired temperature at the inlet of the gas turbine. Oxygen, carbon dioxide, water vapor and nitrogen have also been considered ideal gases. This mixture has been used in the calculations of the cycle; in the modeling of exchangers, pipes and turbomachines, properties of air have been taken as an ideal gas also for exhaust gases.

4.2.2. Supercritical CO_2

Carbon dioxide or R744 possesses highly accurate thermodynamic properties through the fundamental equations developed by Span and Wagner [2]. The conductivity has been determined by Vesovic [3] and is valid for temperatures from 200 °K to 1000 °K and pressures up to 1000 MPa. Finally, viscosity is determined by the studies of Fenghour, Wakeham and Vesovic [4] and is valid for pressures below 300 MPa and temperatures within the range of 200 °K up to 1500 °K.

4.2.3. R-600

The thermodynamic and transport equations used for butane, of molar mass 58.122 g/mol, have been obtained by the program through the studies of Miyamoto and Watanabe [5]. In addition, the equations of state of this fluid are valid for temperatures between 134,87 °K (triple point temperature) and 589 °K and pressures up to 69 MPa. Finally, the conductivity is given by the studies of Perkins, Ramires, Nieto del Castro and Cusco [6], while the viscosity is provided by Younglove and Ely [7].

4.3. Heat exchanger modeling

The modeling of the exchangers has been carried out using the libraries of the environment "Engineering Ecuation Solver" or "EES", using a different model depending on the type of exchanger used.

4.3.1. Shell and tube, finned tubes and finned plate heat exchangers

These three models of heat exchangers have been dimensioned using the variables of heat exchanger effectiveness (ε) and number of units transferred (NTU). Equations (112) and (113) show the general equations used for the calculation of variable paths, obtained from [8] and [9].

$$\varepsilon = HX(TypeHX\$, NTU, C_1, C_2, Return\$) \quad (112)$$

$$NTU = HX(TypeHX\$, \varepsilon, C_1, C_2, Return\$) \quad (113)$$

The TypeHX$ variable is used to specify the flow configuration of the exchanger (parallel flow, cross flow, shell and tubes, etc.); NTU is the ratio between the overall conductance and the minimum capacitance of the exchanger; C1 and C2 are the capacitance ratio of fluids, calculated as the product of mass flow (ṁ) and specific heat (Ce).

It should be noted that these exchanger models do not have a significant variation in properties as they are hardly affected by changes in solar radiation, which simplifies their sizing.

4.3.2. PCHE heat exchangers

As explained in "*Power conversion system for solar thermal tower plant based on Brayton cycle of supercritical CO_2*" [20], PCHE exchangers have been modeled by an iterative process, in which a continuous variation in the properties of the fluid is assumed and its length is divided into minor elements. From a constructive point of view, PCHEs are supplied in modules, which have certain limitations imposed by the manufacturing process:

- The size limitation of each module is 0.6 m x 0.6 m x 1.5 m (width x length x height).
- Each module contains 96000 channels, 48000 for each of the fluids.
- Up to 14 modules can be stacked in a single structure, obtaining a maximum length of 8.4 m.
- The canals are semicircular and have 2 mm in diameter. The distance between each row of channels is 1.5 mm.

To perform the calculation of PCHE heat exchangers, equations (114) and (115), highlighting the following abbreviations:

- i: element to be analyzed.
- Ui: heat transfer coefficient.
- Qi: heat transferred.
- Pi: area of heat transfer obtained through the perimeter.
- Li: length.
- fi: friction factor.
- Δpi: pressure variation.
- Di: hydraulic diameter of the channel.
- ci: fluid velocity.
- ρi: density of the fluid.

$$Q_i = U_i \cdot L_i \cdot P_i \cdot \left(T_{h,i} - T_{c,i}\right) \quad (114)$$

$$\Delta p_i = f_i \cdot \frac{L_i}{D_i} \cdot \rho_i \cdot \frac{c_i^2}{2} \quad (115)$$

The calculation process establishes a number of initial channels, from which the length necessary to transfer the heat and the load losses produced is determined. The number of channels is increased if the maximum pressure loss is above the prescribed, or reduced otherwise. The correlations for convection coefficients are detailed in [10].

It will be assumed that the heat exchangers work at the nominal point and, in addition, their design will be optimized in cases where the mass flow is maximum. It will be also assumed that, despite the complete variation of mass flow that changes in solar radiation entail, variations in CO_2 flow properties are hardly non-existent, so the working conditions of the exchangers will remain constant at all times.

4.4. Pre-design of turbomachines

The sizing of the turbomachines consists of three steps. First, the specific speed (Ns) must be established using Baljè's method [11], which allows the identification of the type of turbomachine to be used inside each cycle (axial, radial or mixed), as shown in Figure 11. Secondly, specific diameter (Ds) is determined and, simultaneously, the performance of the turbomachines is established as it is a function that depends directly on the parameter Ns. Finally, the diameter of the rotor is established from the specific diameter, which is a fundamental parameter for the construction of the same.

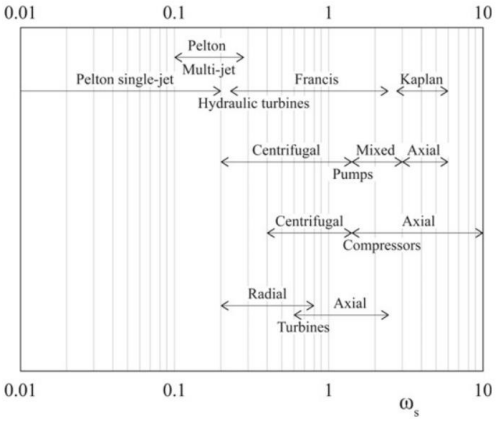

Figure 11: Specific speed of turbomachines. [12]

Turbomachines	Type	Specific speed
Pumps	Radial	0.5÷1.3
	Mixed flow	1.9÷3.0
	Axial	4.0÷5.0
Hydraulic turbines	Pelton	0.04÷0.1
	Francis	0.5÷2.0
	Kaplan	2.5÷3.5
Compressors	Radial	0.4÷1.0
	Mixed flow	1.0÷2.0
	Axial	1.5÷2.5
Turbines	Radial	0.4÷0.8
	Axial	0.6÷1.2

Figure 12: Specific speed ranges to obtain high efficiencies in turbomachines. [12]

To calculate the specific velocity (116) it is necessary to know the angular velocity (w), the volumetric flow (V) and the difference of isentropic enthalpies between the input and the output (ΔHad). If the difference in enthalpies is such that the values of Ns obtained are very low, turbomachines will be introduced in series or the rotational speed of the turbomachine will be increased to increase its specific speed(117); if the Ns is excessively large, the rotational speed of the turbomachine could be modified by decreasing it, or by adding others in parallel, so that, as with the enthalpy difference, the volumetric flow will also be reduced. It should be noted that, in case of introducing several turbomachines in series, it is necessary to calculate the specific speed (116) for each stage, since the Ns is defined for each of them, not for the machine as a whole.

$$N_s = \frac{w \cdot \sqrt{V}}{\left(\Delta H_{ad\_final}\right)^{3/4}} \quad (116)$$

$$\Delta H_{ad\_final} = \frac{\Delta H_{ad}}{n^{o} turbomáquinas} \quad (117)$$

Once the Ns is known, it is necessary to adjust to the parameters established in Figure 12, maximizing the efficiency of the turbomachines. It is possible that for the Ns to be within this range, it

is necessary to introduce one or more turbomachines in series / parallel in order to modify their respective parameters (ΔH_{ad} and V).

After obtaining the specific speed of the turbomachine, an estimate of the maximum performance that each turbomachine will have is obtained simultaneously; therefore, the next step is to establish the specific diameter by using Baljè diagrams [11].

$$\eta = f(N_s, D_s) \quad (118)$$

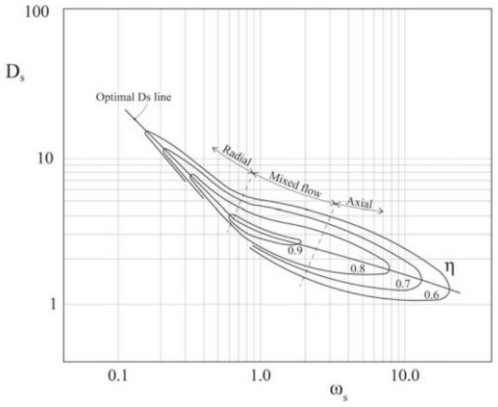

Figure 13: Baljè diagram for pumps. [12]

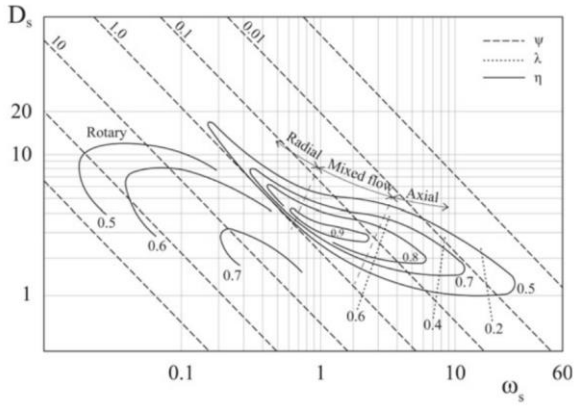

Figure 14: Baljè diagram for compressors. [12]

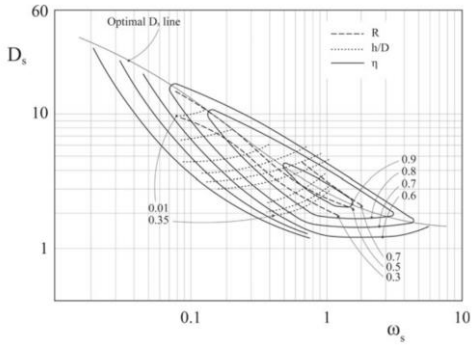

Figure 15: Baljè diagram for axial turbines. [12]

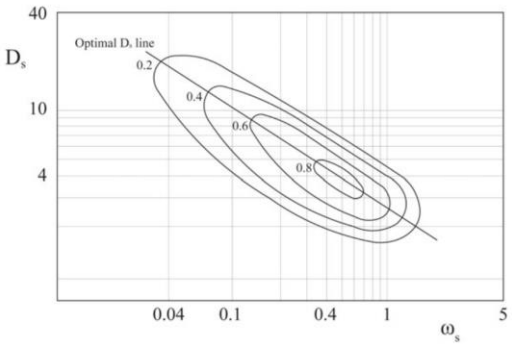

Figure 16: Baljé diagram for radial turbines. [12]

Through the specific diameter, the diameter of the turbomachine rotor (D) is dimensioned, which depends on the adiabatic difference of enthalpies between the inlet and the output of the stage (ΔH_{ad}) and the volumetric flow (V).

$$D_s = \frac{D \cdot \left(\Delta H_{ad\_final}\right)^{1/4}}{\sqrt{V}} \quad (119)$$

Ultimately, in order to limit the centrifugal force of the turbomachines, a maximum peripheral speed value of 450 m/s has been established for them, which is calculated through the rotational speed, w [rad/s] and the rotor diameter, D [m].

$$450\frac{m}{s} > u = w \cdot \frac{D}{2} \quad (120)$$

Particularly, the S-CO_2, gas and R-600 turbines together with the air compressor, have been sized taking into account the variation in density they suffer at the input/output of each stage when several turbomachines are introduced in series. In the case of the S-CO_2 compressor and the R-600 pump, this process has not been necessary since the variation in densities is negligible along the turbomachine.

4.5. Pipe design

The pipes are the elements responsible for transporting the fluid around the cycle, therefore, it is necessary to ensure its operation and guarantee its resistance to the high pressure and temperature loads of the plant. In addition, they must be properly insulated thermally and acoustically. To carry out its sizing it has been decided to use two different criteria:

- Firstly, the criteria of maximum permissible speed have been established, avoiding possible problems related to noise and vibration. With it, if the fluid is in a gaseous state, the limitation shown in equation (124). However, if the fluid has low density, its maximum velocity shall be limited in such a way that it does not exceed 60 m/s in the case of a gas, or 6 m/s if it is a liquid.
- In the second instance, the criteria of loss of load has been established, in such a way that the values established by the regulations are not exceeded. These values limit the pressure loss in 3 different segments (only valid for fluids in the gaseous state):
    - If the pressure is greater than 138 bar.

$$Pérdida_{CargaMáx} = \frac{p}{500} \quad (121)$$

    - If the pressure is between 138 bar and 35 bar.

$$Pérdida_{CargaMáx} = (p - 35) \cdot \frac{(0{,}27 - 0{,}11)}{(138 - 35)} + 0{,}11 \quad (122)$$

    - If the pressure is less than 35 bar.

$$Pérdida_{CargaMáx} = p \cdot \frac{(0{,}11 - 0{,}001)}{(35 - 0)} + 0{,}001 \quad (123)$$

For the sizing of the plant, three different pipe materials have been used according to the fluids that circulate through each of the cycles. In the case of the gas cycle, the "310s Alloy" [13] has been used (formed by austenitic stainless steel for high temperature applications, with great resistance to corrosion and a high content of Nickel and Chromium), since it can withstand temperatures of up to 1038 °C without seeing its properties diminished. For the S-CO_2 cycle and for the ORC cycle, it has been decided to use the Inconel 740-H pipes, formed by an alloy of Ni-Cr-Co. Finally, for the cooling circuit, whose working fluid is water, A-106B (carbon steel) pipes will be used.

The nomenclatures and formulas used during the sizing of the pipes are as follows.

Nomenclatures:

- Pressure: p [bar].

- Temperature: T [orC].
- Density: ρ [kg/m3].
- Viscosity: μ [m2/s].
- Mass flow: ṁ [kg/s].
- Number of pipes: n [-].
- Fluid velocity: v [m/s].
- Pipe diameter: D [mm].
- Pipe internal diameter: d [mm].
- Maximum permissible voltage: S [MPa].
- Pipe thickness: t [mm].
- Reynolds number: Re [-].
- Roughness: ε [mm].
- Friction factor: f [-].
- Coefficient y: and [-].

Formulas:

$$v_{max} = 175 \cdot \left(\frac{1}{\rho}\right)^{0,43} \quad (124)$$

$$D_{min} = 1000 \cdot \sqrt{\frac{4 \cdot \dot{m}}{n \cdot \pi \cdot \rho \cdot v_{max}}} \quad (125)$$

$$t_{min} = \frac{T \cdot 100 \cdot D_o}{2 \cdot (S \cdot 1000 + T \cdot 100 \cdot y)} \quad (126)$$

$$d = D_o - 2 \cdot t \quad (127)$$

$$v = \frac{\dot{m}}{n \cdot \rho \cdot \left(\pi \cdot \frac{d}{1000}\right)^{2/4}} \quad (128)$$

$$Re = v \cdot \frac{d}{1000 \cdot \mu} \quad (129)$$

$$\frac{h_f}{L} = \frac{1000 \cdot f \cdot v^2}{d \cdot 2 \cdot 9,81} \quad (130)$$

$$\frac{1}{\sqrt{f}} = -2 \cdot log\left(\frac{\varepsilon/d}{3,7} + \frac{2,51}{Re \cdot \sqrt{f}}\right) \quad (131)$$

The sizing of the pipes has been carried out through an iterative process that begins by introducing the working conditions of the pipes at each of the points of the cycle. The variables that are necessary to know to carry out this analysis are pressure, temperature, density, viscosity and mass flow.

Once the working conditions are known, the number of pipes is chosen and, by means of the criteria of maximum permissible speed, a normalized diameter value (D_N) is established, higher than the minimum diameter (D_{min}) calculated through the equation (125) Next, the thickness of the

pipe is decided, greater than the minimum thickness [equation (126)], calculated through the ASME/ANSI B36.10 M standard [14]. In case of either, there are no standard pipes wide enough to be able to transport the fluid, or that the thickness of the pipe is insufficient, pipes will be added in parallel to, in this way, be able to divide the mass flow that will circulate through the pipes and, consequently, reduce its diameter and thickness.

After having dimensioned through the criterion of maximum permissible speed, the criterion of maximum pressure loss will be applied, by means of which the pressure loss of each of the pipe sections will be calculated using the Darcy-Weisbach equation [equation (130)] and the friction factor of the Colebrook equation [equation (131)]. If the pressure loss is greater than the value recommended by the Norsok standard [18], the pipe diameter or the number of pipes must be modified until the pressure drop has an acceptable value.

5. Results

This section shows the performance obtained by the system against the variability of solar input, keeping the conditions of the input air and refrigeration constant. In this sense, it can be understood as obtaining the benefits in nominal point depending on the solar contribution. In addition to the performance, the dimensions established for each of the elements that make up the plant will also be obtained.

5.1. Cycles

As previously mentioned, the addition of the solar receiver next to the heat recuperator of the gas turbine, cause variations in the gas consumption requested by the plant depending on the solar radiation absorbed. Consequently, this also causes a decrease in emissions at peak times. Figure 17**¡Error! No se encuentra el origen de la referencia.** shows this variation, observing a linear relationship between both variables, emissions and consumption of natural gas with solar radiation, which shows that at times when this is non-existent the plant consumes about 125 g CH_4 / kWhe and emits into the atmosphere about 345 g CO_2 / kWhe, while at times when it is maximum, the plant goes on to consume about 85 g CH_4/kWhe and emit approximately 235 g CO_2/kWhe, which translates into a reduction of up to 32% in natural gas consumption and CO_2 emissions.

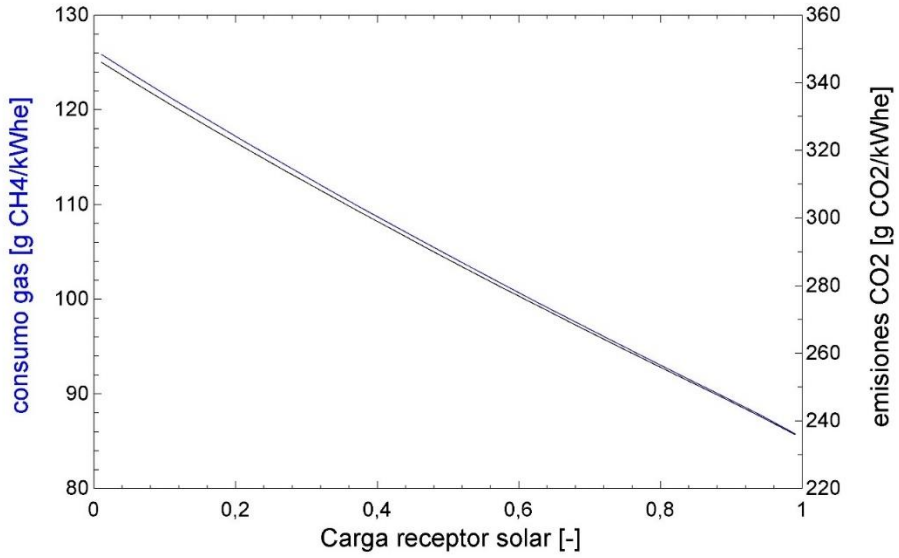

Figure 17: Variation in natural gas consumption and CO_2 emissions emitted as a result of solar radiation.

However, the variation of the energy generating method (natural gas or natural gas + solar receiver) causes variations in the performance of the combined cycle, which produces modifications in the amount of energy produced. Figure 18 shows how cycle efficiency is minimized when the plant operates in extreme conditions (minimum or maximum solar radiation), while maximum performance is achieved at times when the solar receiver load is at 50%. However, the loss of efficiency suffered by the combined cycle under both extremes of operation is not significant, since it varies only by 1.1% (corresponding to the minimum yield of 56.85% and the maximum 57.5%). On the other hand, the net energy produced by the combined cycle reaches its maximum value when there is no energy contribution from the solar receiver, this being 182.8 MWe, and, being the minimum value under load conditions of the solar receiver of approximately 83%, producing the plant 177 MWe. Finally, it should be noted that under a condition of 100% charge by the solar receiver the electrical power generated is 178 MWe.

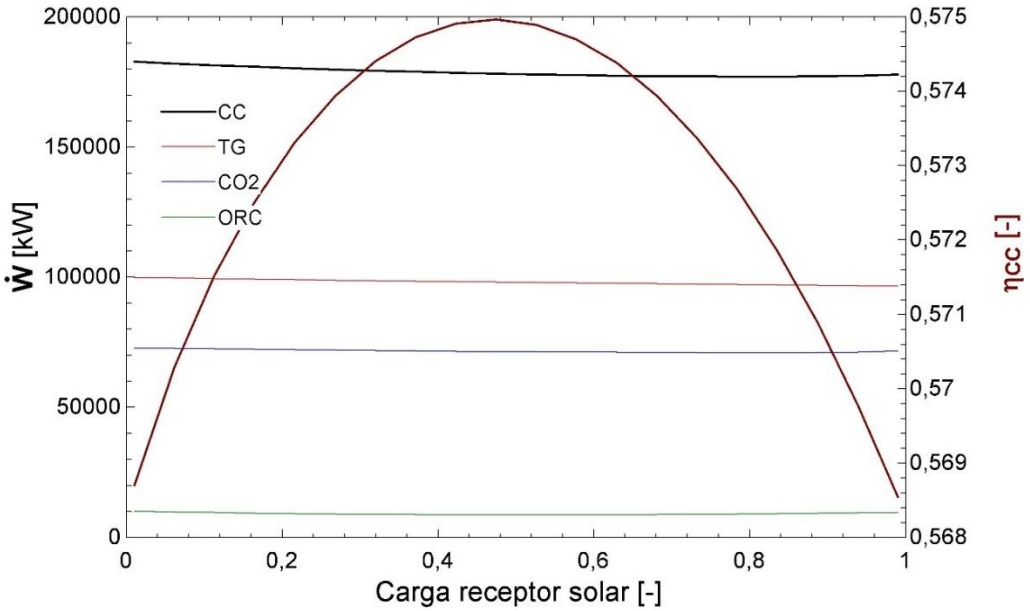

Figure 18: Variation of the energy obtained in each of the cycles and the performance of the combined cycle depending on the load of the solar receiver.

5.1.1. Variations in the operation of the elements of the gas cycle depending on the load of the solar receiver

Within the gas cycle, the main element that undergoes variations in its point of work is the regenerator of the gas turbine, for which two different scenarios have been analyzed. First, Figure 19 shows how the heat exchange between the cold current (compressor outlet and inlet to the combustion chamber) and hot current (turbine outlet) takes place, in which, because the hot current has a mass flow 5 times less than the cold current, the energy load of the higher temperature current suddenly decays ($\Delta T_{hot\ current}$ = 500 °C), while the lowest temperature current has a variation of 120 °C, being the amount of energy exchanged by both currents of 24 MW. Secondly, Figure 20 shows a scenario in which the load of the solar receiver corresponds to 80%, which produces that both currents are more balanced in terms of mass flow and, therefore, the heat exchange is higher than the previous case (81 MW) and the relationship between heat exchanged per MW is much more equitable, being 5.13 °C/MW in the case of cold current and 5.19 °C/MW in the case of hot current.

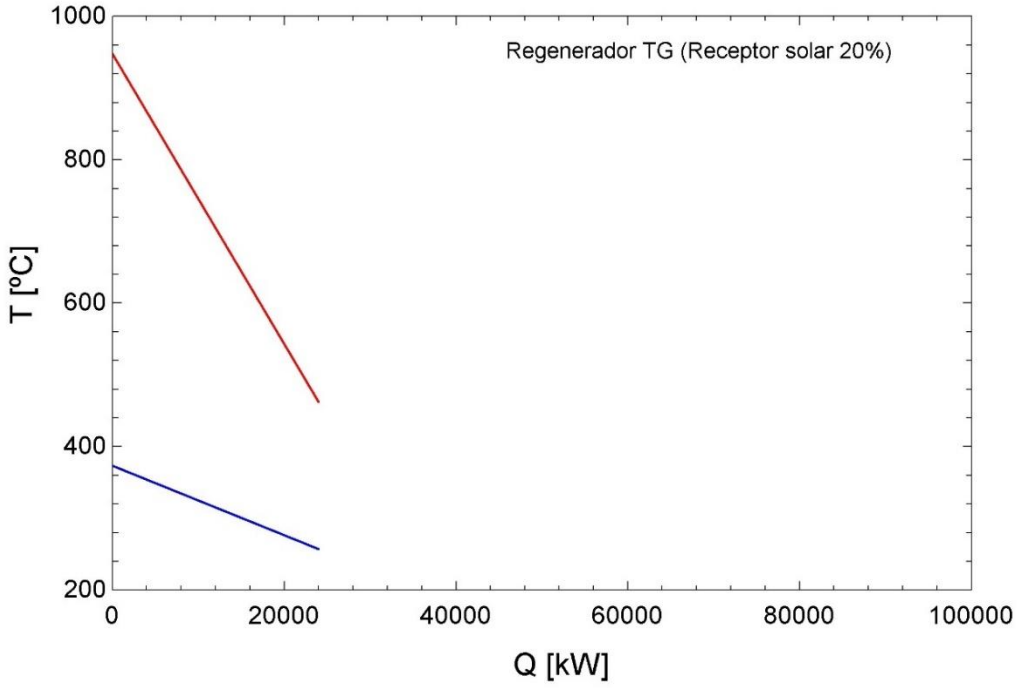

Figure 19: Gas turbine regenerator under a solar receiver load of 20%.

491

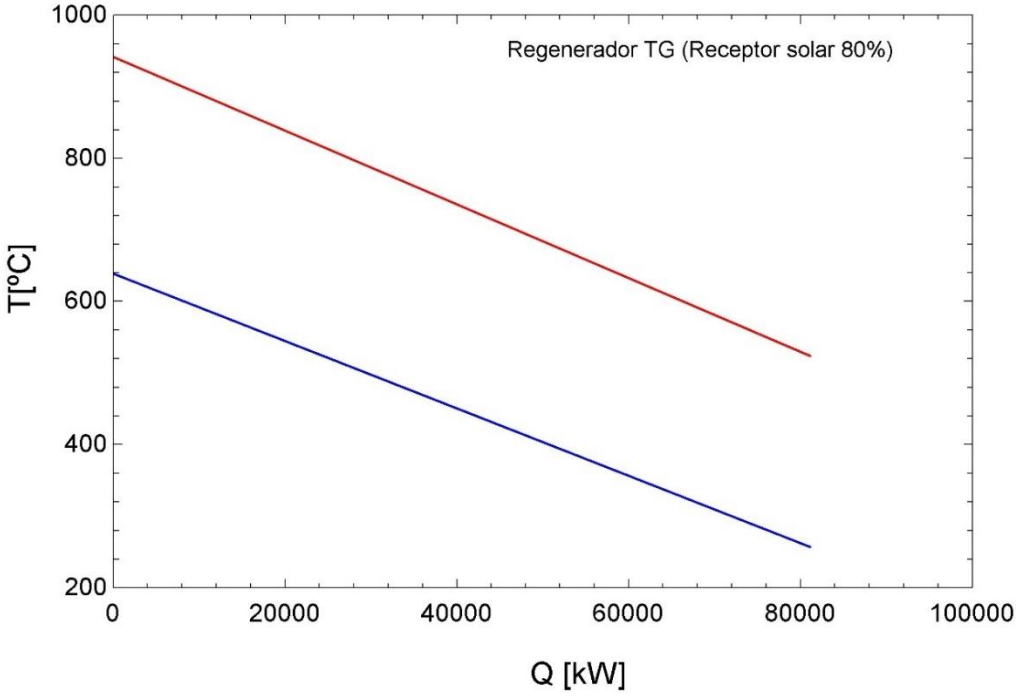

Figure 20: Gas turbine regenerator under a solar receiver load of 80%.

492

Other elements of the gas cycle that are affected by the variation of solar charge are the HTHR and ITHR exchangers. Unlike the gas turbine recuperator, the HTHR exchanger works better with a lower load of the solar receiver, since its mass flow depends inversely on this parameter. Figure 21 shows how both heat exchangers work almost optimally when the degree of charge of the solar receiver is low, also possessing an approach of around 25 °C as shown in Figure 23. On the contrary, Figure 22 shows how the heat exchange of the HTHR exchanger is considerably reduced by decreasing the mass flow that circulates through the hot current, simultaneously reducing the approaching between both flows.

Regarding the ITHR exchanger, it is not so affected by the variation of the solar load, since, being after the union of flows from the output of the gas turbine and the heat recuperator makes its temperature is much more constant than that of the HTHR exchanger, exchanging in both cases approximately the same amount of energy (≈46 MW).

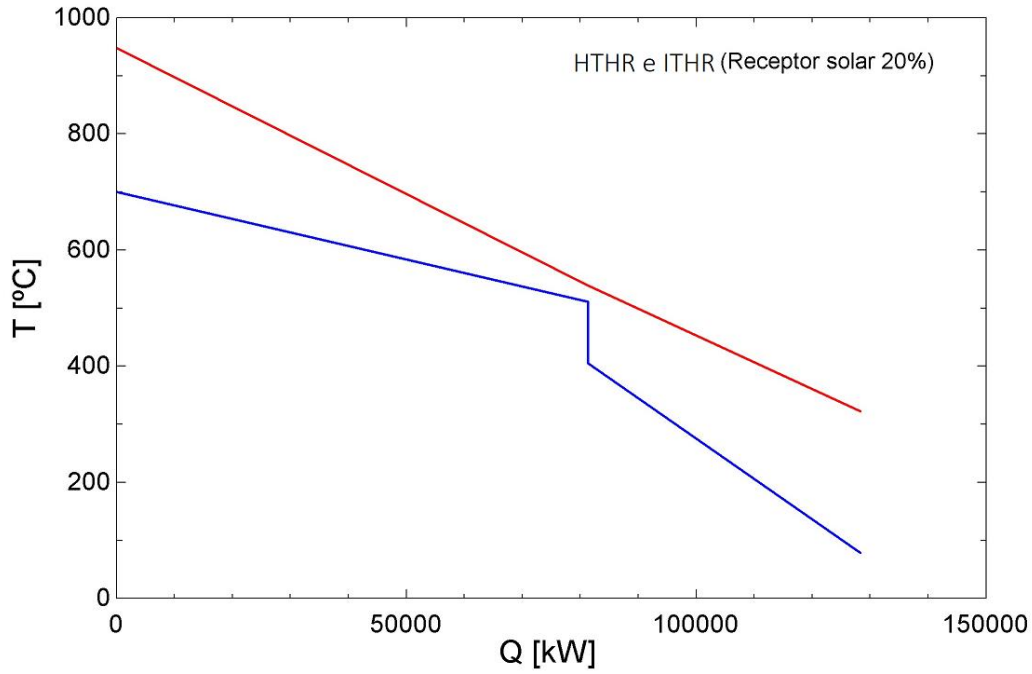

Figure 21: HTHR and ITHR exchangers under a solar receiver load of 20%.

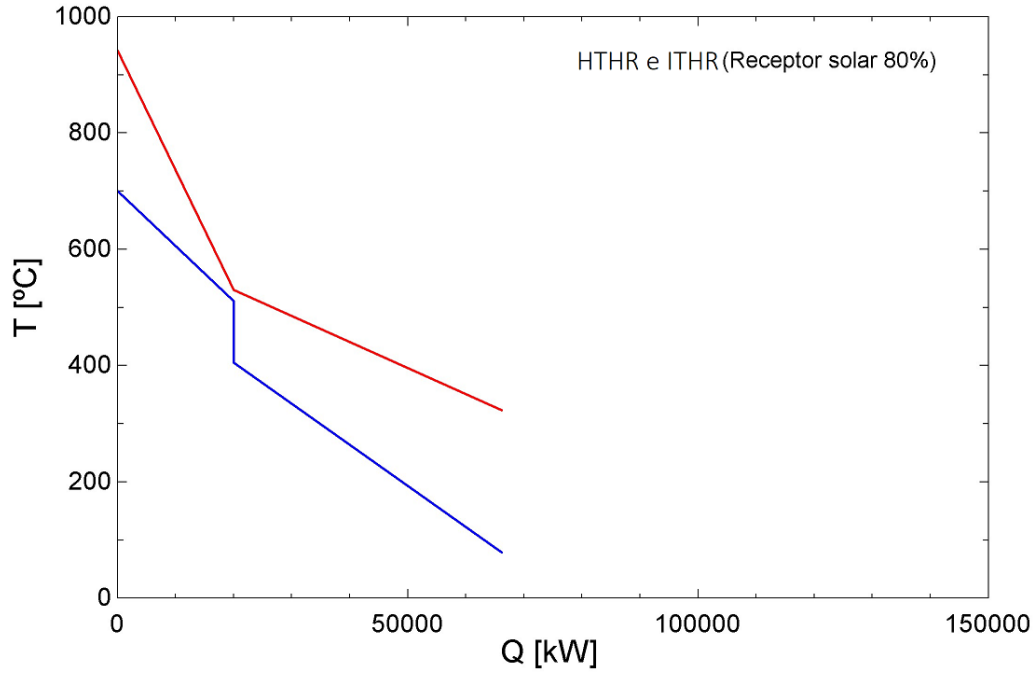

Figure 22: HTHR and ITHR exchangers under a solar receiver load of 80%.

506

507

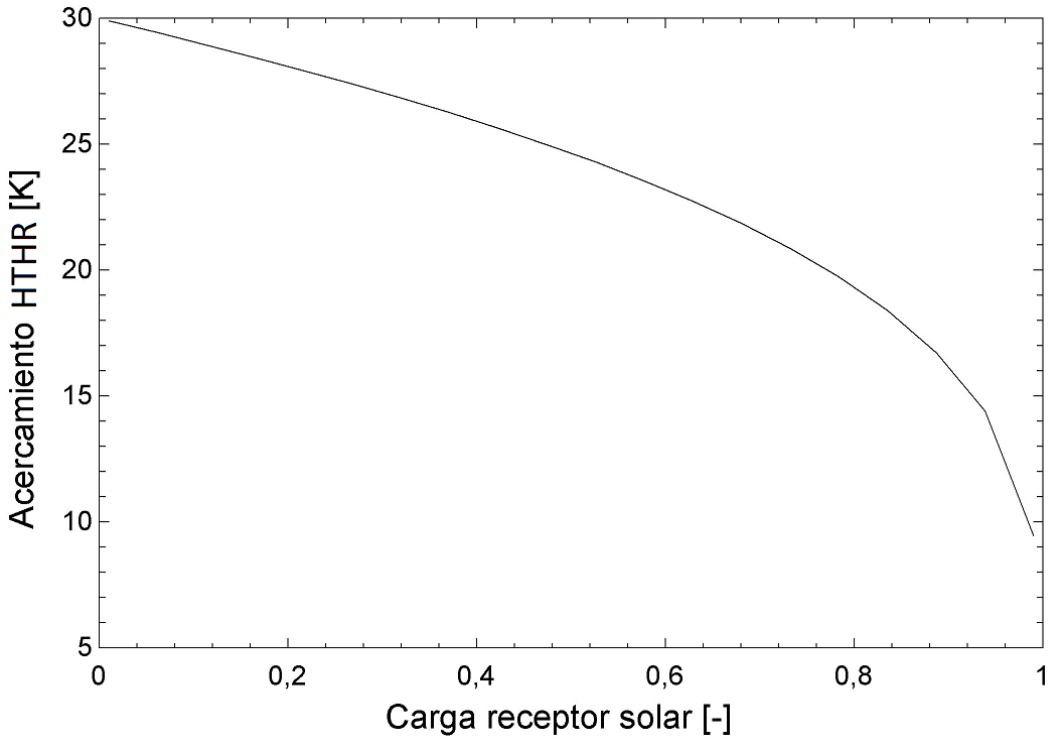

Figure 23: Approach of the HTHR exchanger as a function of the load of the solar receiver.

508

Finally, Figure 24 shows how the output temperatures of the gas turbine recuperator and the HTHR exchanger vary, demonstrating that, as the load of the receiver increases, the recuperator intensifies the amount of energy exchanged by having a greater mass flow by the hot current and, consequently, increases the temperature of the air at its exit. On the other hand, in the case of the HTHR heat exchanger, the opposite happens, as the load of the receiver increases, the temperature at its exit decreases due to the mass flow of the hot current decreases and, as a result, the amount of heat exchanged also decreases.

In Figure 24 it can also be seen that the ITHR exchanger is the one that suffers the least variations when the limit cases are compared; being its entry temperature practically identical, under both the conditions, maximum load by the solar receiver, and under minimum load, the amount of heat it exchanges does not suffer variations. As a particularity, this exchanger has its minimum efficiency when the load of the solar receiver is around 50%, since, as its inlet temperature is minimal, so will be the output temperature.

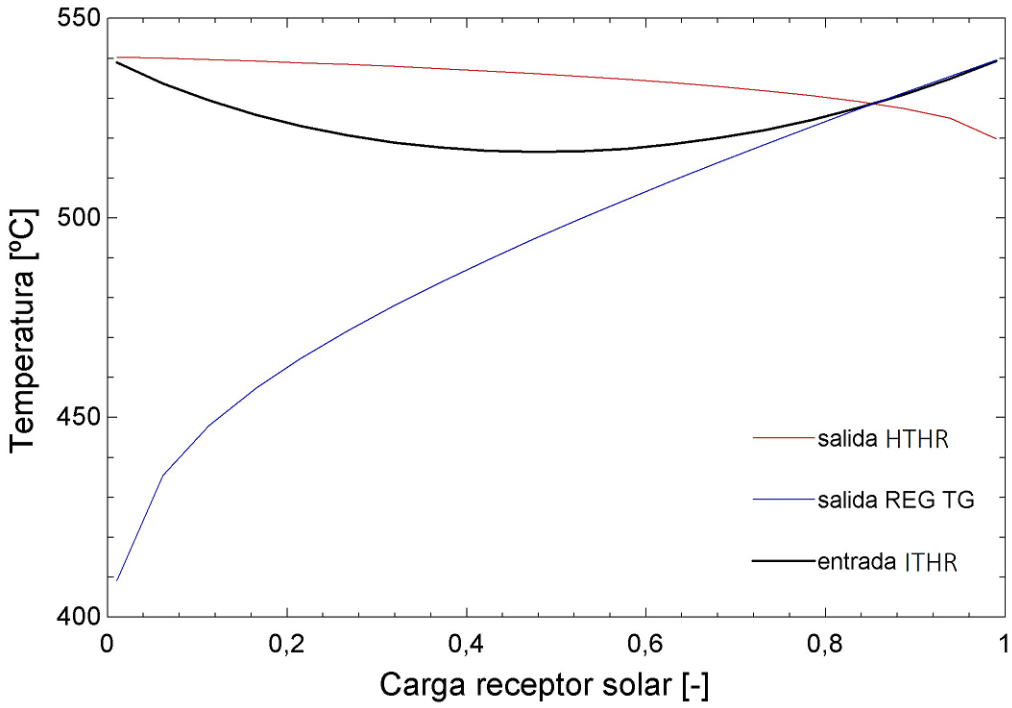

Figure 24: Output temperature of the elements affected by the load of the solar receiver depending on it.

5.1.2. Variations in the operation of the elements of the CO_2 cycle depending on the load of the solar receiver

To facilitate its design and construction, the CO_2 cycle has been divided into two twin units, therefore, all the elements of this cycle will be duplicated, with the only exception of the medium temperature exchanger of CO_2-CO_2, which, when exchanging heat to a small part of the mass flow, will only be connected to one of the currents, rejoining the flows of both cycles before passing through the HTR exchangers.

In reference to the mass flow of the CO_2 cycle, Figure 25 shows how it varies according to the load of the solar receiver, being maximum when the load is non-existent and minimum when its

capacity is around 80%. In addition, it should be noted that when the load capacity exceeds 90%, there is an increase in the need for mass flow by the CO_2 plant. However, for the sizing of all the elements of the cycle, it has been chosen to use the most unfavorable case, that is, the one with the highest mass flow (443.9 kg/s).

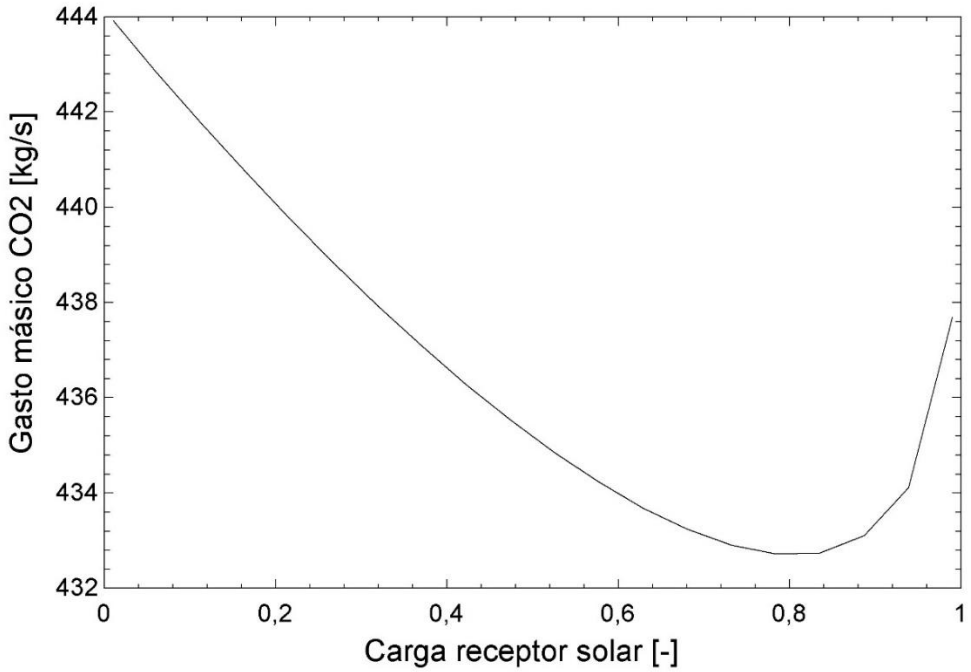

Figure 25: Mass flow of CO2 as a function of the load of the solar receiver.

HTR heat exchangers are the internal element of the CO_2 cycle that undergoes greater variations in its working point due to the load of the solar receiver. The CO_2 cycle has two HTR exchangers that work simultaneously, but with the inverse amount of mass flow, that is, if the HTR heat exchanger of the solar receiver has 80% of the mass flow, the HTR heat exchanger of the gas cycle will have the remaining 20%. Figure 26 and Figure 27 refer to the HTR heat exchanger found behind the HTHR heat exchanger, in other words, the gas cycle.

Another remarkable feature of these exchangers is that, unlike the gas turbine recuperator, when the load of the solar receiver varies, it does not only affect one flow, but both. Therefore, the approach between the two flows, hot and cold, remains approximately constant at all times.

Figure 26 shows that, when the mass flow passing through the exchanger is high (80% of the total mass flow in this case), the amount of power exchanged is also very high, specifically in this case 110 MW. On the other hand, Figure 27, referring to a small amount of mass flow (20%), causes the power exchanged by the heat exchanger to be much lower than the previous case (of the order of 27 MW). In addition, as previously mentioned, since both mass flows are similar, it can be observed how the approach of the exchanger hardly varies.

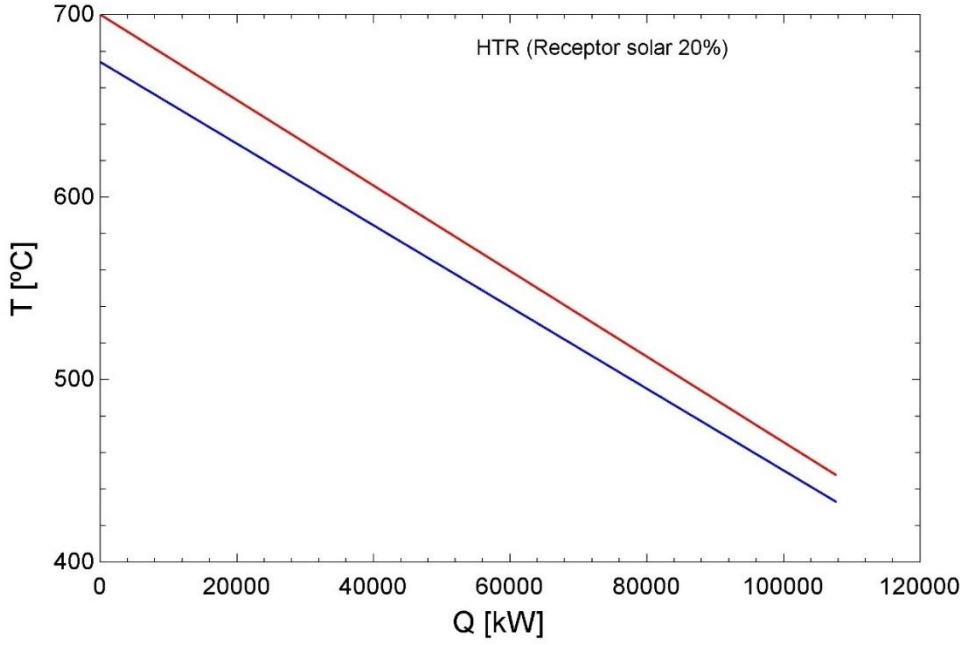

Figure 26: HTR (gas) exchanger under a solar receiver load of 20%.

554

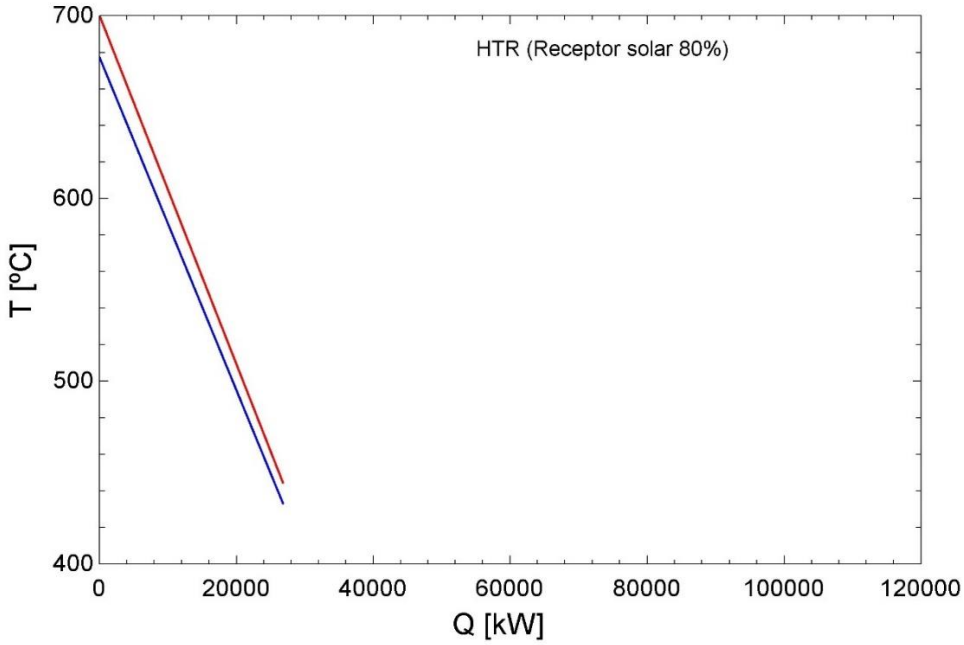

Figure 27: HTR (gas) exchanger under a solar receiver load of 80%.

555

556

5.1.3. Variations in the operation of the elements of the ORC cycle depending on the load of the solar receiver

The ORC cycle is the one in which fewer variations occur due to the load of the solar receiver, since the main variation it has is its inlet temperature. The temperature is directly related to the inlet temperature of the ITHR exchanger (Figure 24), so, it has its minimum when the load of the solar receiver is approximately 50% and its maximum when the receiver operates at its extremes, which causes the efficiency of the ORC cycle to decrease slightly when it is under the first operating condition mentioned. Finally, the most characteristic point to analyze in Figure 28 is the exhaust temperature of the gases from the ORC boiler, that is, those coming from the gas turbine. As mentioned in the previous sections, to avoid possible problems related to corrosion (condensation of acidic products) the ideal is that the temperature of these gases does not decrease below 100 °C. However, in order to maximize the efficiency of the cycle, the temperature of these gases has been allowed to decrease to 95 °C for the receiver charge range from 25% to 75%, since the combined cycle will operate most of the time outside this range, where the gases will reach temperatures of up to 114 °C (in the case of zero load).

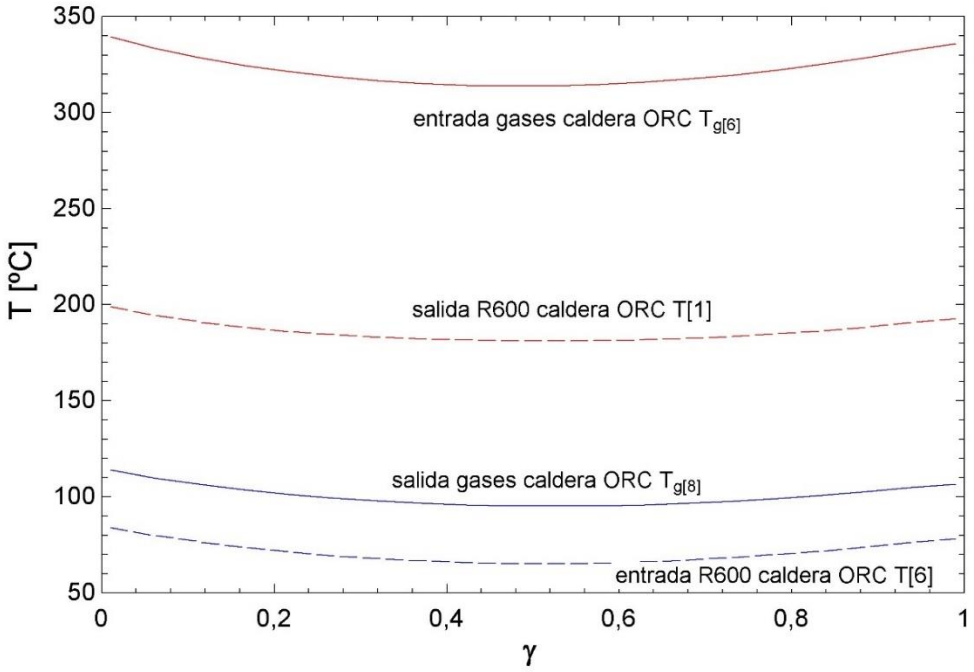

Figure 28: Operating temperature of the ORC cycle elements as a function of the load of the solar receiver.

5.2. Heat exchangers

Heat exchangers have been designed to cope with the working point that produces a greater load. Therefore, for some of the operating points discussed in the previous section, these exchangers will be oversized.

First, **¡Error! No se encuentra el origen de la referencia.** the cross-flow heat exchangers. As is normal, the HTHR heat exchanger is the one with the highest heat exchange, since, of the three

exchangers, this is where the fluid circulates at the highest temperature. Consequently, this exchanger is also the one with the largest dimensions. However, because the S-CO_2 cycle has been divided into two twin units, this exchanger has been separated into two units of identical dimensions (**¡Error! No se encuentra el origen de la referencia.**).

Within the cross-flow exchangers, the one with the smallest size is the ITHR, since the amount of CO_2 that circulates inside it is much lower than that of the HTHR. In addition, although the temperature of the inlet air is higher compared to the LTHR, its power is lower, since this exchanger does not need to transfer to the CO_2 cycle as much heat as the LTHR to the ORC cycle.

Table 1: Dimensions of cross-flow exchangers.

Cross-flow exchangers		
HTHR	Power [MW]	93,3
	Height [m]	12,31
	Width [m]	3,25
	Length [m]	0,50
	Volume [m^3]	20,12
	nº tubes	12300
ITHR	Power [MW]	43,3
	Height [m]	5,27
	Width [m]	4,75
	Length [m]	0,32
	Volume [m^3]	7,89
	nº tubes	3300
LTHR	Power [MW]	46,8
	Height [m]	4,57
	Width [m]	6,35
	Length [m]	0,63
	Volume [m^3]	18,22
	nº tubes	5700

Table 2: HTHR exchanger divided into two twin units.

2xHTHR	Power [MW]	46,6
	Height [m]	6,16
	Width [m]	3,25
	Length [m]	0,50
	Volume [m^3]	10,1
	nº tubes	6150,0

Secondly, **¡Error! No se encuentra el origen de la referencia.** shows the dimensions and power of t he finned plate exchanger, the gas turbine regenerator. Because the air represents both working fluids of the exchanger, its volume is much higher than the rest of the plant heat exchangers that do not produce a phase change.

Table 3: Dimensions of the finned plate exchanger.

Plate exchanger with fins		
Regenerador TG	Power [MW]	90,3
	Height [m]	5,23
	Width [m]	2,05
	Length [m]	11,08
	Volume [m^3]	119
	n° plates	445

Thirdly, **¡Error! No se encuentra el origen de la referencia.** shows the characteristics of the shell a nd tube exchanger, which is responsible for condensing the R-600 fluid. The fluids that will pass through its interior will be water (as a refrigerant) and R-600, in a gaseous state at the entrance and in a liquid state at the outlet.

Table 4: Dimensions of the shell and tube exchanger.

Shell and tube exchanger		
ORC Capacitor	Power [MW]	37,4
	Housing diameter [m]	5,91
	Length [m]	10,39
	Volume [m^3]	284,83
	n° tubes	35000

Finally, **¡Error! No se encuentra el origen de la referencia.** shows the dimensions of the PCHE exchangers, which have as constructive restrictions their length, which cannot exceed 8.5 m (14 modules) and their height (1.5 m). Therefore, it is necessary to divide them into different sections so that heat exchange occurs optimally. As with the HTHR heat exchanger, HTR, LTR and PC heat exchangers have been divided into two twin units, one for each of the supercritical CO_2 cycles (**¡Error! No se encuentra el origen de la referencia.**). Figures 29 to 33 show how these exchangers will be built.

Table 5: Dimensions of PCHE exchangers.

PCHE exchangers		
HTR	Power [MW]	133,4
	Height [m]	1,78
	Width [m]	0,6
	Length [m]	12,62

	Volume [m^3]	13,42
	n° modules	22
LTR	Power [MW]	197,6
	Height [m]	4,49
	Width [m]	0,6
	Length [m]	15,03
	Volume [m^3]	40,5
	n° modules	26
PC	Power [MW]	77,0
	Height [m]	0,49
	Width [m]	0,6
	Length [m]	8,50
	Volume [m^3]	2,24
	n° modules	15
Regenerador ORC	Power [MW]	12,6
	Height [m]	0,97
	Width [m]	0,6
	Length [m]	8,76
	Volume [m^3]	5,09
	n° modules	15
Loop Cycle: Exchanger CO_2-CO_2	Power [MW]	47,0
	Height [m]	4,44
	Width [m]	0,6
	Length [m]	3,94
	Volume [m^3]	10,49
	n° modules	7

614

Table 6: HTR, LTR and PC exchangers divided into two twin units. 615

HTR	Power [MW]	66,7
	Height [m]	1,78
	Width [m]	0,60
	Length [m]	6,31
	Volume [m^3]	13,42
	n° modules	11
LTR	Power [MW]	98,783
	Height [m]	4,50
	Width [m]	0,60
	Length [m]	7.5 0
	Volume [m^3]	40,5
	n° modules	13

PC	Power [MW]	38,5
	Height [m]	0,5
	Width [m]	0,60
	Length [m]	4,25
	Volume [m^3]	2,24
	n° modules	7,5

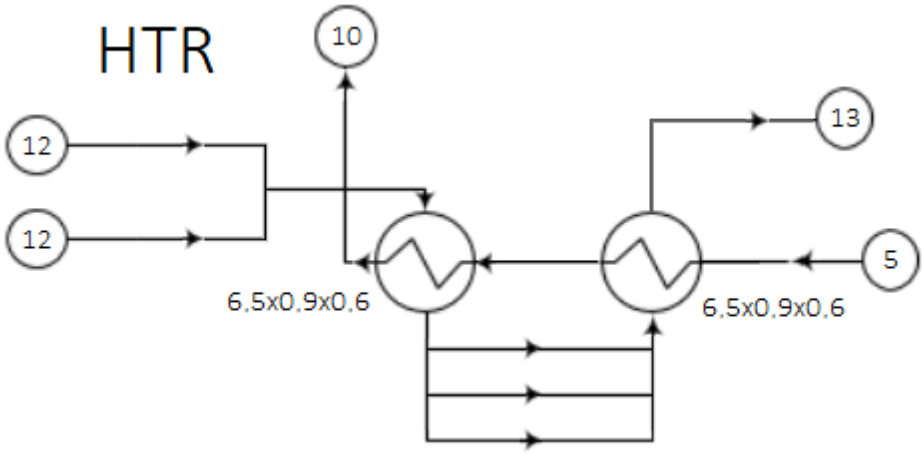

Figure 29: Design of an HTR heat exchanger unit.

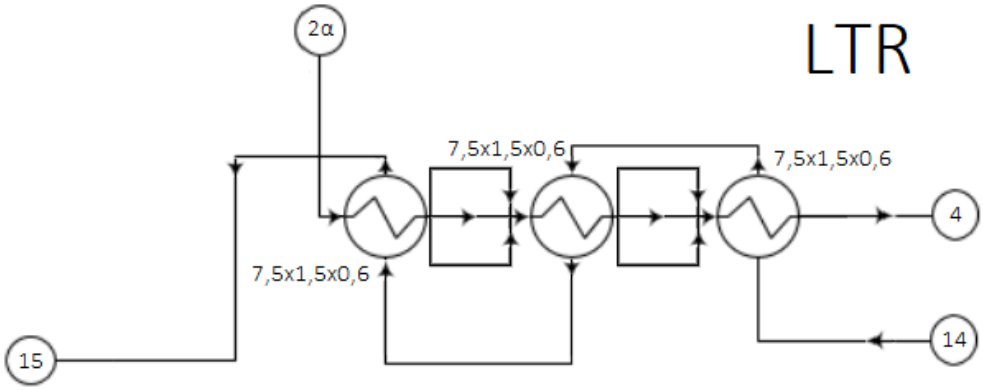

Figure 30: Design of an LTR heat exchanger unit.

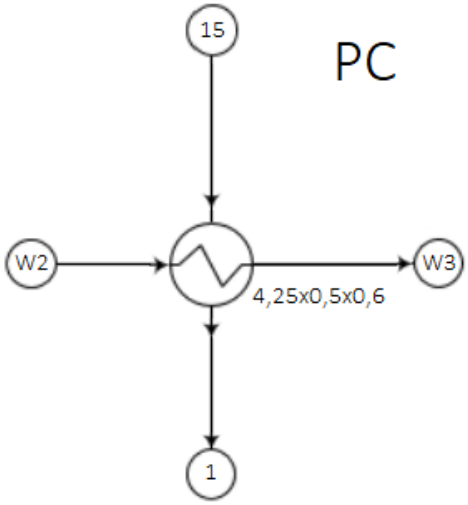

Figure 31: Design of a PC heat exchanger unit.

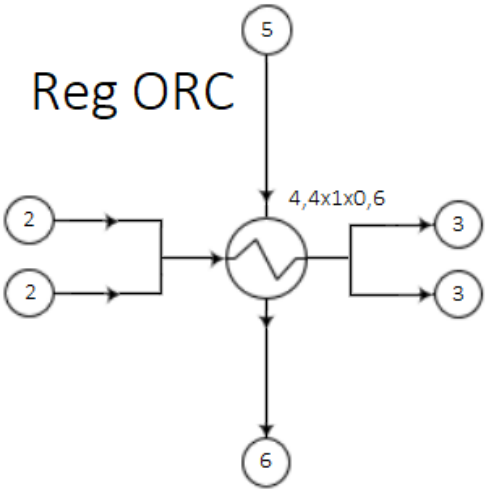

Figure 32: Design of a Reg ORC heat exchanger unit.

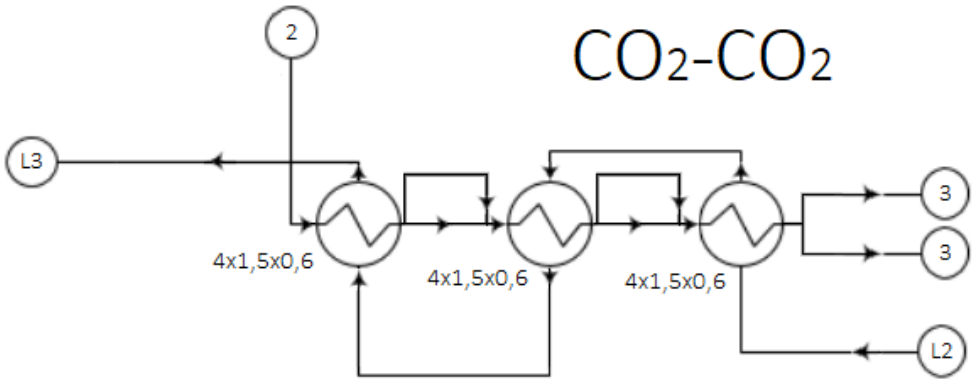

Figure 33: CO_2-CO_2 heat exchanger design.

5.3. Turbomachines

Because the plant is composed by three types of cycles with their respective fluids (air, CO_2 and R-600), it has been decided to use a different synchronism speed for each of the cycles. In addition, in all cases both turbomachines, compressor (or pump in the case of the R-600) and turbine, will be coupled to the same shaft and, therefore, will have the same rotational speed.

Every turbine used at the plant will be axial turbomachines, so will be the gas cycle compressor. In contrast, the S-CO_2 cycle compressor and the ORC cycle pump will be radial turbomachines. Table**¡Error! No se encuentra el origen de la referencia.** shows the data and operating characteristics of each of the turbomachines.

Table 7: Data on input and output conditions of turbomachines.

Cycle type	Type of turbomachine	T° input [°C]	P entrance [bar]	T° output [°C]	P exit [bar]
Gas cycle	Axial Turbine	674,1	299,2	510,4	86,6
	Axial Compressor	35	85	72,55	300
CO_2 cycle	Axial Turbine	1500	6,752	940,1	1
	Radial Compressor	15	1	257	6,752
ORC Cycle	Axial Turbine	198,9	50	108,4	3,29
	Radial Pump	35	3,29	39,43	50

It should be noted that, in the case of compressors, the stages that have the highest specific speed are those that are at the beginning, since the fluid has a lower density and, therefore, its flow rate is higher. In turbines the opposite happens, the first stages are corresponding to those with the highest Ns, since, as the temperature and pressure of the fluid decrease, density of is also reduced at the exit of each stage, which produces lower Ns values compared to the previous stages.

5.3.1. Gas cycle

Air has a density that varies significantly depending on pressure and temperature. Therefore, in order to establish the number of stages that the turbomachine will have, an analysis has been carried out in which its density variation is taken into account at the output / input of each of the stages. In addition, it is necessary to optimize the number of stages in such a way that the performance of each of the turbomachines coupled in series is maximized, which forces to limit the specific speed within the range of Ns ∈ [0,6 - 1,2] for the axial turbine and Ns ∈ [1,5 - 2,5] for the axial compressor.[52]

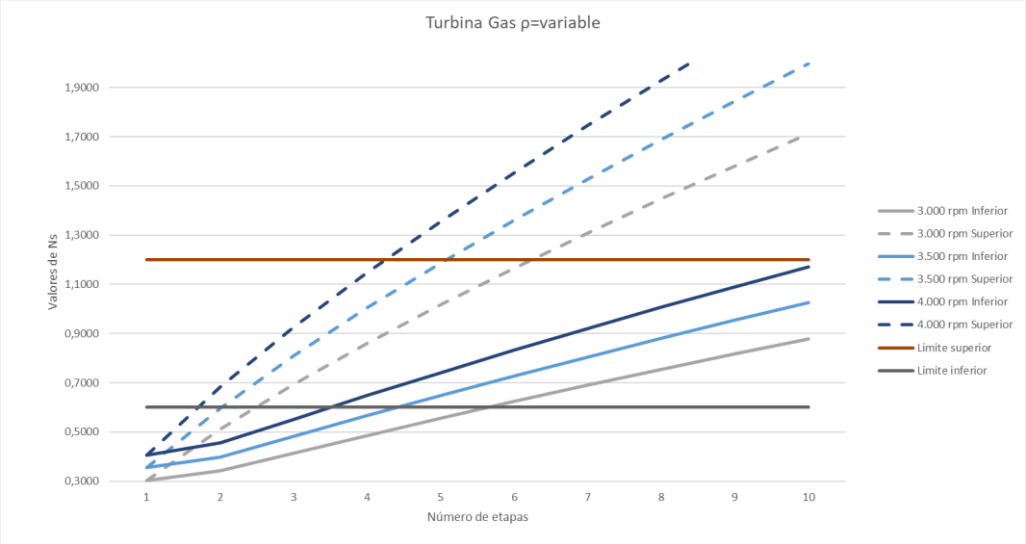

Figure 34:Variation of the Ns as a function of the number of stages of the gas turbine.

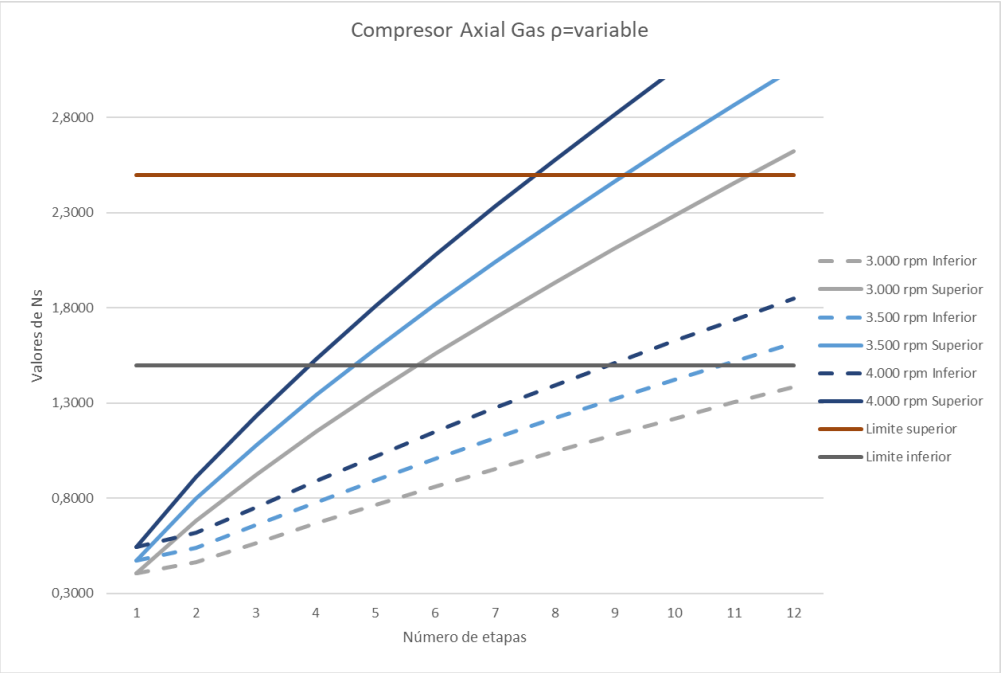

Figure 35: Variation of the Ns depending on the number of stages of the gas compressor.

Looking at Figure 34 and Figure 35, it has been decided that the rotational speed of the gas turbomachines is 3000 rpm, since this is the synchronism speed of the Spanish electrical system. Consequently, it is necessary to use at least 6 stages for the turbine, since in this way all the stages are within the limits marked by the Ns, and 11 or 12 stages for the compressor. It has been decided to finally use 11 stages because the performance of axial compressors decreases to a greater extent when exceeding the upper limit than if the lower limit is not reached. With all this, the results shown in **¡Error! No se encuentra el origen de la referencia.** and Table 1.

Table 8: Sizing of the gas compressor stages.

Sizing of gas compressors				
	Rotational speed [rpm]	η [-]	D [m]	u [m/s]
Stage 1	3000	0,89	2,59	407,23
Stage 2	3000	0,9	2,49	391,72
Stage 3	3000	0,9	2,31	363,49
Stage 4	3000	0,9	2,24	352,16
Stage 5	3000	0,9	2,18	342,03
Stage 6	3000	0,9	2,04	320,92
Stage 7	3000	0,9	1,99	313,28
Stage 8	3000	0,9	1,88	295,68
Stage 9	3000	0,9	1,84	289,78
Stage 10	3000	0,9	1,75	274,83
Stage 11	3000	0,9	1,72	270,19

Table 1: Sizing of the gas turbine stages.

Sizing of gas turbines				
	Rotational speed [rpm]	η [-]	D [m]	u [m/s]
Stage 1	3000	0,92	2,44	383,46
Stage 2	3000	0,92	2,64	414,37
Stage 3	3000	0,92	2,78	436,68
Stage 4	3000	0,91	2,74	430,33
Stage 5	3000	0,9	2,78	437,17
Stage 6	3000	0,89	2,82	442,41

5.3.2. S-CO_2 cycle

Because CO_2 has very high densities in the areas near its critical point, in the case of the compressor, it has been decided not to take into account the variation in density between stages, since it is insignificant. On the other hand, the turbine, having a higher temperature and, consequently, lower density, has been analyzed from both perspectives in order to optimize its design, showing in Figure 37 the case without variation in density between stages and in Figure 38 the opposite.

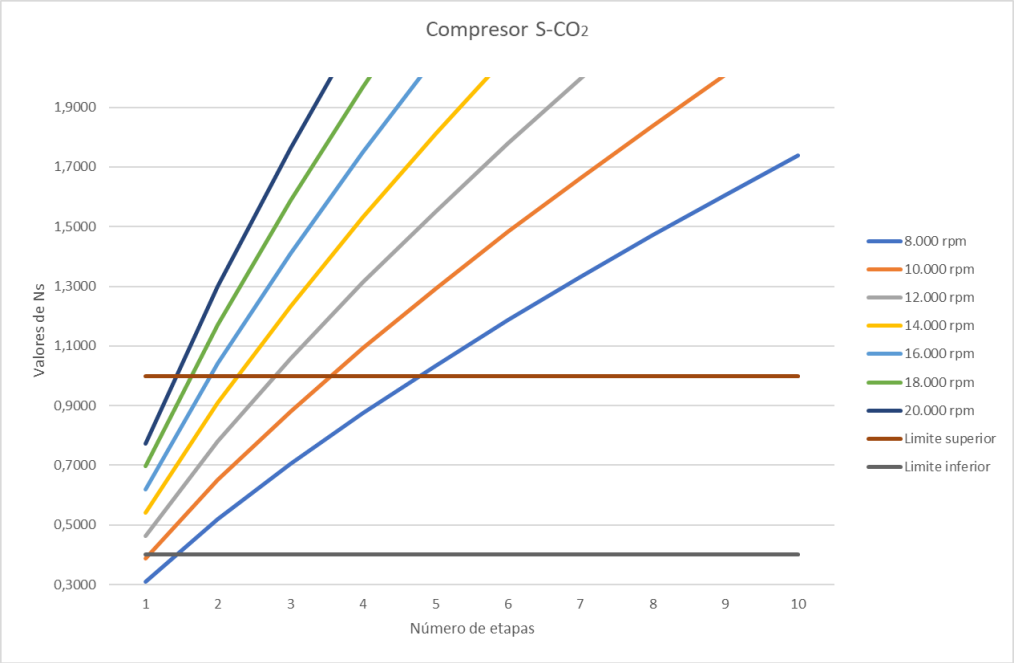

Figure 36: Variation of the Ns as a function of the number of stages of the S-CO2 compressor with constant density.

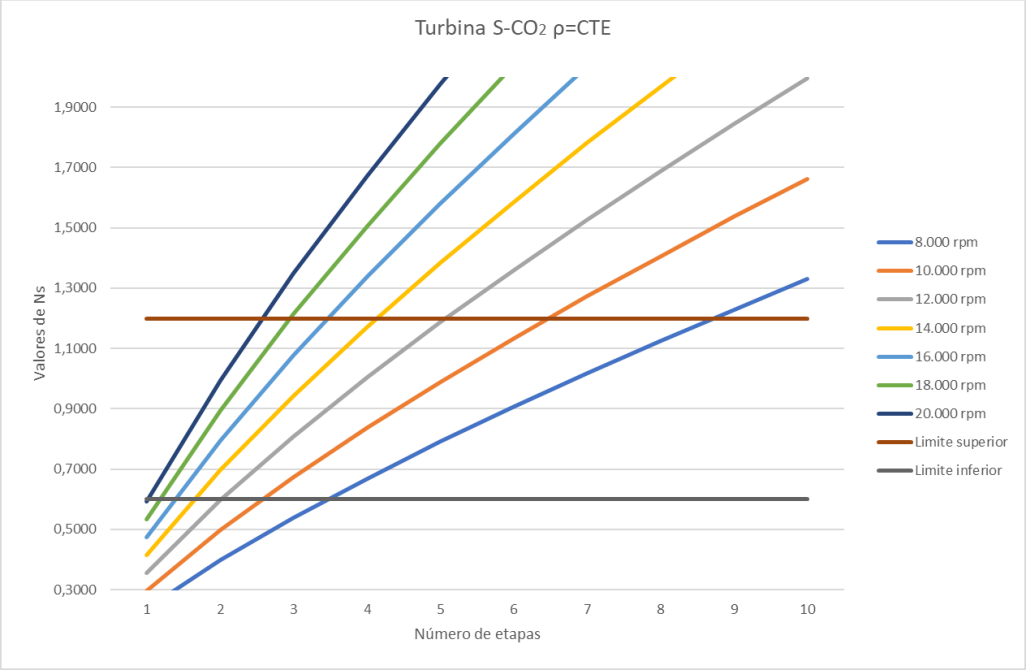

Figure 37: Variation of the Ns as a function of the number of stages of the S-CO_2 turbine with constant density.

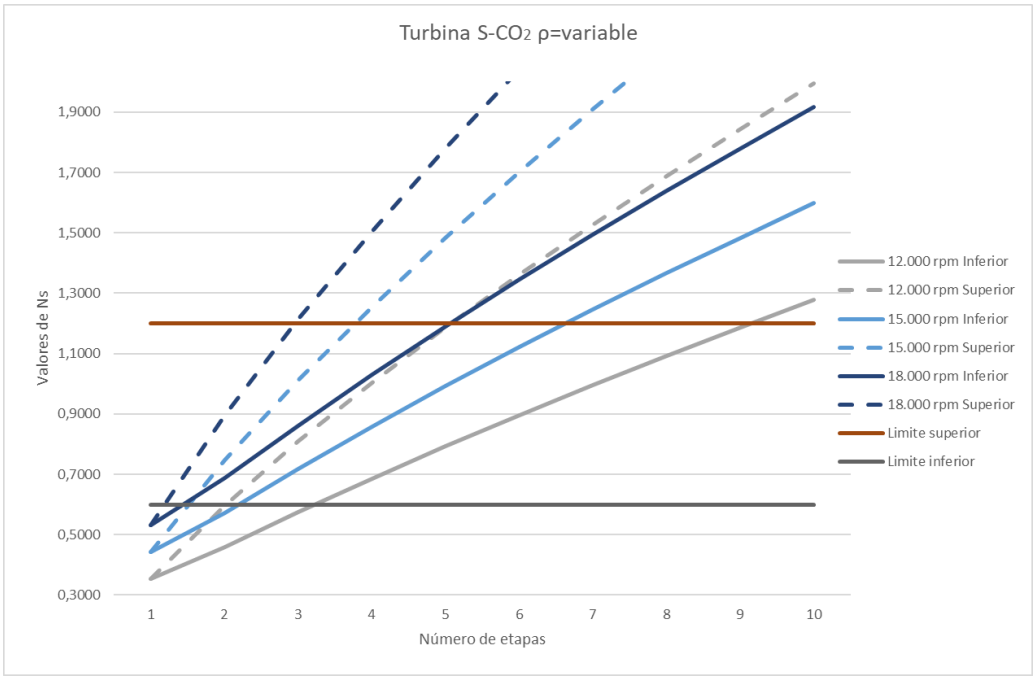

Figure 38: Variation of the Ns as a function of the number of stages of the S-CO_2 turbine with variable density.

As **¡Error! No se encuentra el origen de la referencia.** shows, the CO_2 compressor, which is a radial compressor, is within the limits of the Ns for speeds from 12000 rpm to 20000 rpm using a single stage. On the contrary, the turbine is more limited with respect to the speed it must have if a single

stage is used, so, in order to optimize the performance of the plant, it has been decided to finally use 2 stages with a rotational speed of 18000 rpm for both turbomachines.

Table 2: S-CO_2 turbomachine sizing.

Sizing of CO_2 turbomachines				
	Rotational speed [rpm]	η [-]	D [m]	u [m/s]
Compressor	18000	0,9	0,258	243,003
Turbine stage 1	18000	0,92	0,399	376,028
Turbine stage 2	18000	0,92	0,458	432,092

Table 2 shows the sizing of the CO_2 cycle turbomachines. In it, it can be seen that the yields of all turbomachines are above 90% (92% in the case of turbines) and that in no case is the limit of 450 m/s established as a limit for centrifugal force is exceeded.

5.3.3. ORC Cycle

As in the previous cases, the number of turbine stages has been calculated through the variable density criteria. However, for the pump, as the fluid is in a liquid state and, therefore, it is an incompressible fluid, it has not been necessary to apply this criterion. This results in the graphs shown in Figure 39 and Figure 40.

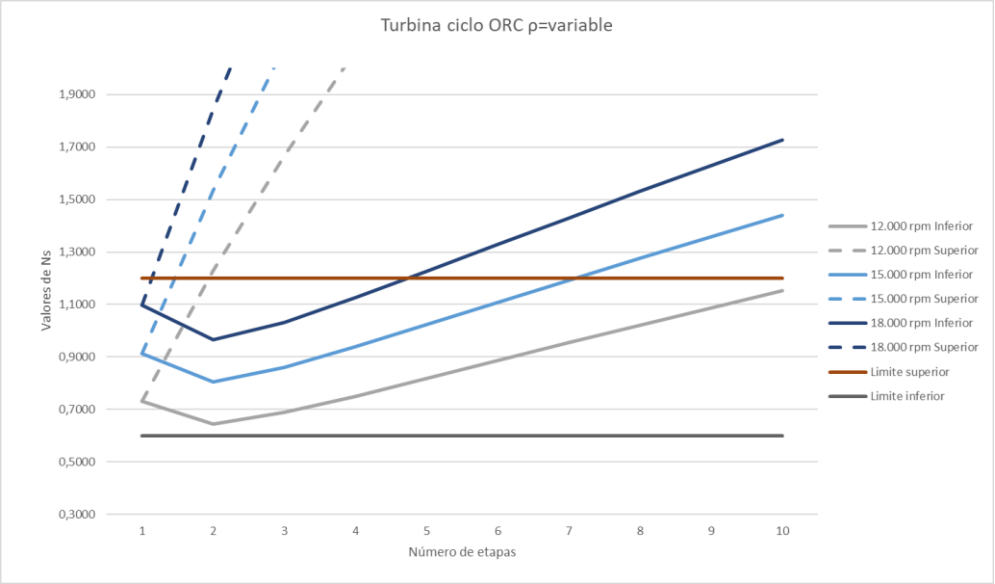

Figure 39: Variation of the Ns as a function of the number of turbine stages of the ORC cycle.

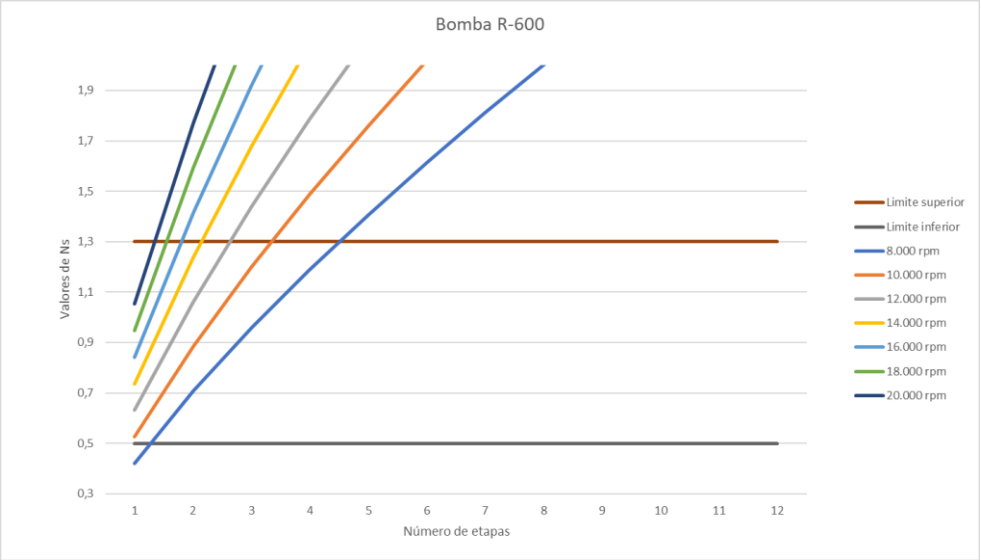

Figure 40: Variation of the Ns as a function of the number of pump stages of the ORC cycle.

In both graphs it can be seen that for rotational speeds between 12000 rpm and 18000 rpm both turbomachines are within the established limits and, in addition, only a single stage is needed for each of them. So finally, a rotational speed of 12000 rpm has been chosen in such a way that the centrifugal force that the turbomachines must withstand is minimized.

Table 3: Sizing of the turbomachines of the ORC cycle.

Sizing of the turbomachines of the ORC cycle.				
	Rotational speed [rpm]	η [-]	D [m]	u [m/s]
Turbine	12000	0,92	0,68	425,33
Bomb	12000	0,9	0,18	114,90

Table 3 shows the performance and impeller dimensions of both turbomachines. In addition, it can be verified that in both cases the maximum value of 450 m/s is not exceeded.

5.4. Pipes

Tables 12 to 15 show the dimensions of the pipes used for the combined cycle. It should be noted that in the case of the CO_2 cycle, the ORC cycle and the water cycle all the pipes are standardized, while, in the gas cycle, due to the high viscosity of the air and its low density, they have not been standardized, since there are no standardized pipes of that size, and, instead, ones with the dimensions set out inTable 5. Finally, it should be noted that in point 3 of the air pipes, outlet of the combustion chamber and inlet of the turbine, it is not necessary to size any pipe since both components are directly coupled to each other.

Table 4: Sizing of CO_2 pipes.

S-CO_2				
Point	nº pipes	DN	schedule	Standard
1	2	350,00	20	YES
2	1	200,00	80	YES
2_alpha	2	250,00	80	YES
3	2	200,00	80	YES
4	2	350,00	80	YES
5	2	400,00	100	YES
6	2	450,00	120	YES
7	2	550,00	20	YES
8	4	450,00	40	YES
9	2	550,00	20	YES
10	2	450,00	140	YES
11	2	450,00	120	YES
12	4	450,00	40	YES
13	2	550,00	20	YES
14	2	550,00	20	YES
15	2	450,00	20	YES
L1	1	350,00	20	YES
L2	1	450,00	20	YES
L3	1	400,00	20	YES

Table 5: Sizing of air pipes.

Air				
Points	nº pipes	Do(mm)	t(mm)	Standard
1	1	2400,00	1,00	NO
2	1	1300,00	2,00	NO
3	---	---	---	---
4	2	2800,00	2,00	NO
5	2	2300,00	1,00	NO
5p	2	2300,00	1,00	NO
5m	2	2300,00	1,00	NO
6	2	2100,00	1,00	NO
7	2	1000,00	3,00	NO
8	2	1900,00	1,00	NO

Table 6: Sizing of R-600 pipes.

R-600				
Points	nº pipes	DN	schedule	Standard
1	1	400,00	20	YES
2	4	650,00	STD	YES
3	4	650,00	STD	YES
4	1	500,00	20	YES
5	1	300,00	20	YES
6	1	300,00	20	YES

Table 7: Sizing of water pipes.

Water				
Points	nº pipes	DN	schedule	Standard
PC_1	6	400	20	YES
PC_2	6	400	20	YES
PC_3	6	400	20	YES
C_ORC_1	1	700	20	YES
C_ORC_2	1	700	20	YES
C_ORC_3	1	700	20	YES

Figures 41 to 46 show the diagrams of the cycles with the indication of the number of pipes, their nominal diameter and their thickness. For the CO_2 cycle and for the pipes connecting the gas cycle exchangers to it, they have been given an even number of pipes as the carbon dioxide cycle has been divided into two twin units.

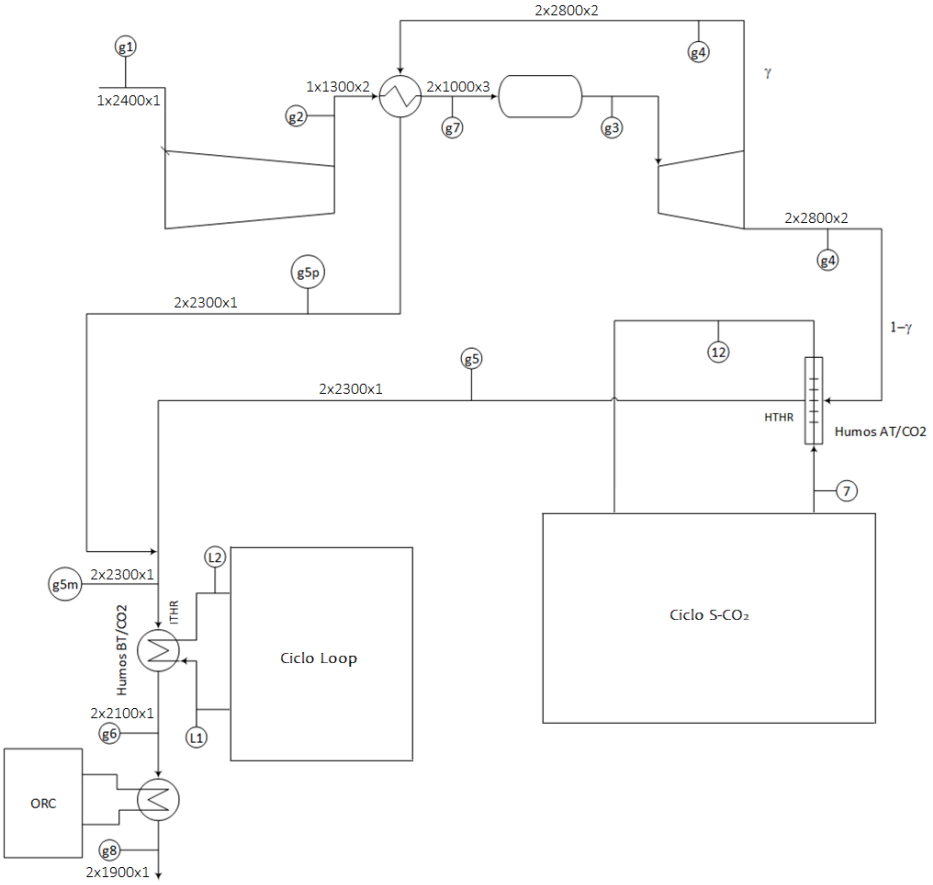

Figure 41: Diagram of the gas cycle with the pipeline design.

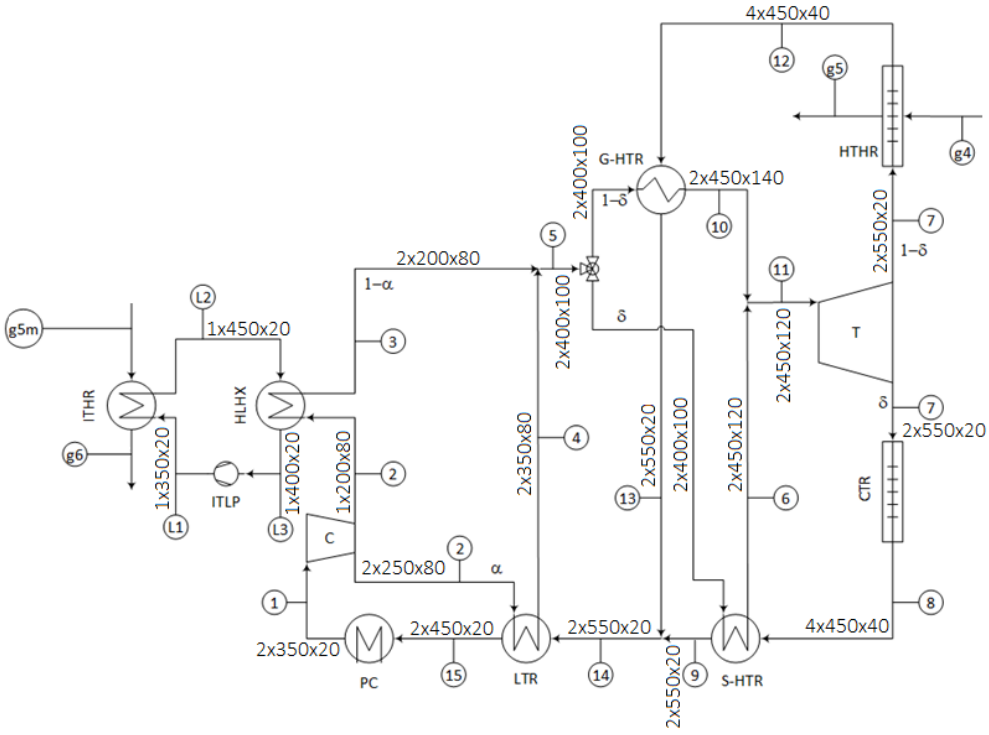

Figure 42: Diagram of the CO_2 cycle with pipes.

727

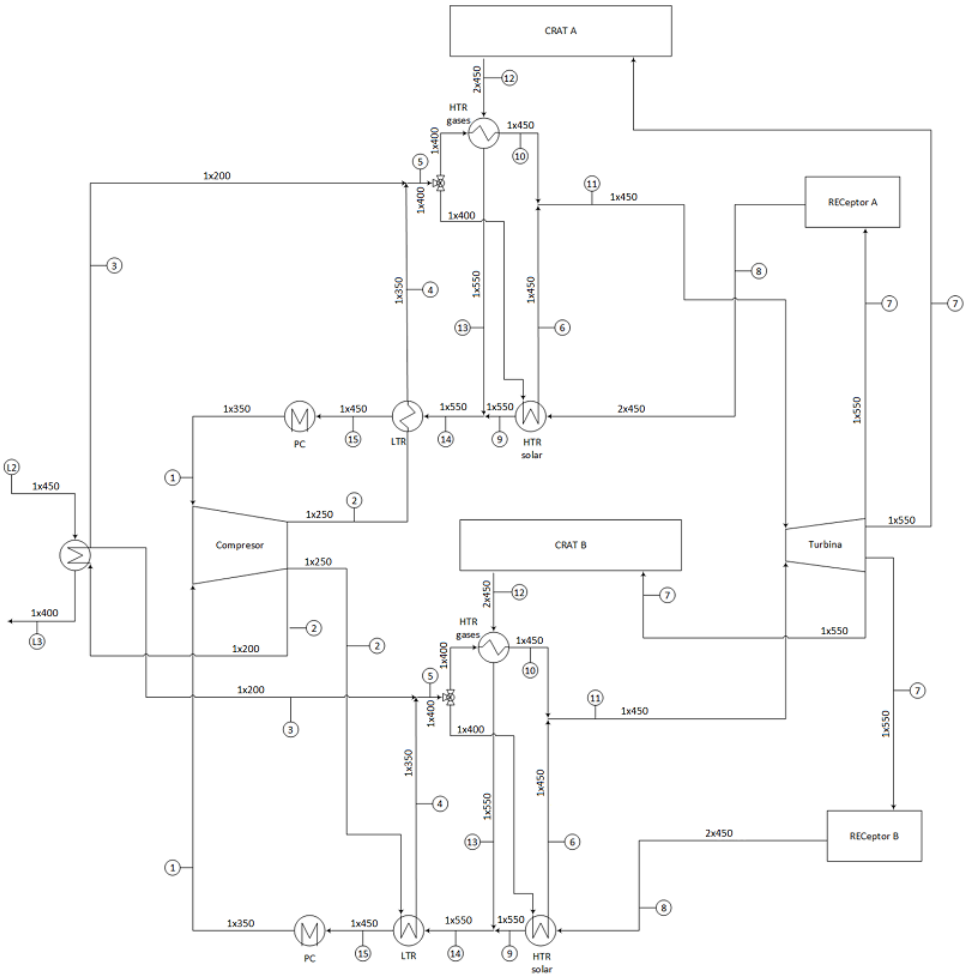

Figure 43: Diagram of the CO_2 cycle divided into two parallel cycles with pipes.

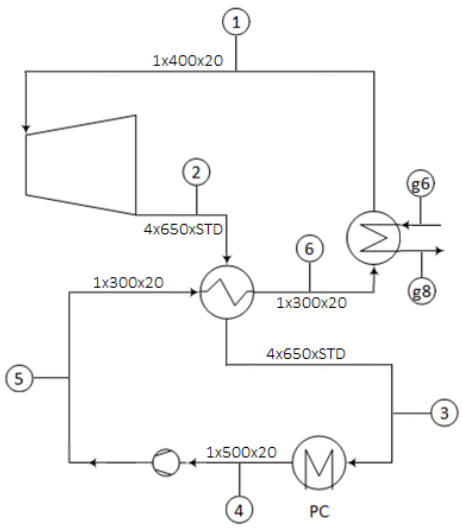

Figure 44: Diagram of the ORC cycle with pipes.

728

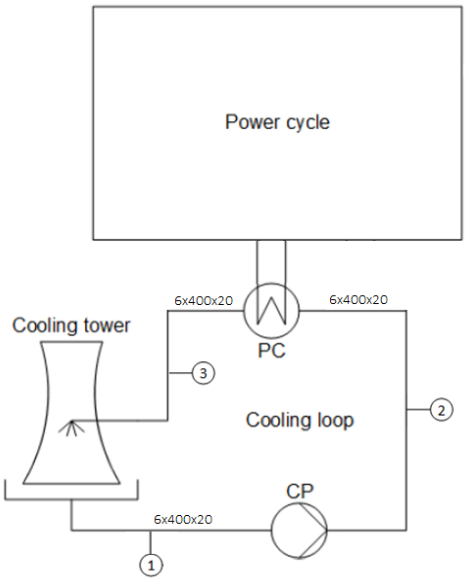

Figure 45: Diagram of the CO_2 cooling cycle.

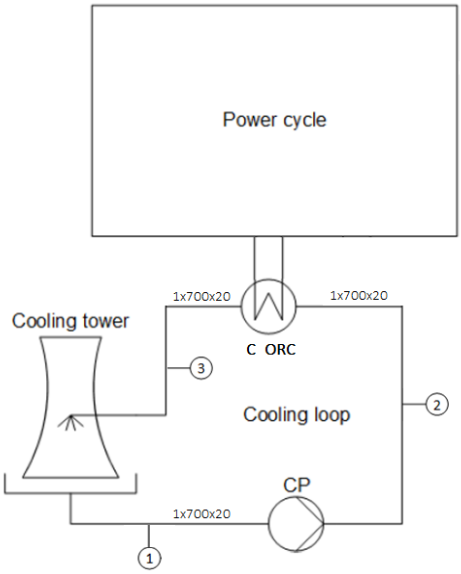

Figure 46: Diagram of the ORC cooling cycle.

6. Conclusions

A new energy generation alternative has been proposed that allows the use of renewable energy sources and that is capable of operating when renewable resources are non-existent. The project presents the 48ybridization of a combined cycle with an S-CO2 cycle as a bottoming cycle, supported by a solar tower receiver and an ORC cycle. The plant has been studied under constant ambient and cooling conditions, with a variable solar contribution. This modelling maintains an almost constant energy output of 180 Mwe with an average efficiency of 57.2%. In addition, it can reduce its emissions by up to a third thanks to the support of the solar tower receiver.

Finally, there are various alternatives to replace natural gas as a fuel, such as hydrogen, biomethane or gasified biomass, which would allow this model of thermal power plant to be 100% renewable. Furthermore, it is also possible to keep the use of solar thermal energy practically constant with the implementation of a molten salt storage system.

Appendix A- Sustainable Development Goals

Among the objectives established in the SDGs, the main ones that are achieved in this project are two:

- 7. Affordable and non-polluting energy: with the implementation of combined cycle hybridization of natural gas with solar thermal energy, it is possible to reduce the amount of fuel used during the intermediate hours of the day and, consequently, the environmental impact that occurs is considerably reduced. On the other hand, by having the gas turbine to increase the capacity factor without oversizing the heliostat field, it is expected to considerably reduce the LCOE. In addition, in case of implementing sustainable fuels such as green hydrogen or biomethane, it will be possible to obtain an energy generation method completely aligned with the 2050 agenda, of a manageable nature, which will allow it to be used as an energy backup.

- 13. Climate action: with the reduction of natural gas consumption, the amount of CO_2 emitted into the atmosphere is reduced, reducing the greenhouse gases generated. Likewise, if technologies such as CO_2 capture are implemented, this generation method would become completely sustainable, and if, in addition, renewable gases are added to the equation, it could even help the decarbonization of the atmosphere, by generating negative emissions.

Figure 47: SDG 7, affordable and clean energy. [15]

Figure 48: SDG 13, climate action. [15]

Secondarily, the implementation of this technology also applies to other objectives such as:

- 11. Sustainable cities and communities: with the reduction of emissions in the generating environment, more sustainable communities are achieved, allowing other sectors such as mobility (through plug-in or electric hybrid cars) or industry (such as steel through technologies such as EAF or electric arc furnace, which depend directly on the method of energy generation) to become zero emissions.
- 14. Underwater life: by reducing the amount of natural gas used, it is possible to reduce some impacts on the aquatic environment such as ocean acidification or marine ecotoxicity.
- 15. Life of terrestrial ecosystems: in the same way as with underwater life, the impacts on terrestrial ecosystems are also diminished by impacts such as deforestation or terrestrial ecotoxicity. In addition, the use of biomethane allows the circular economy to be applied, generating fertilizers from digestate.

Figure 49: SDG 11, sustainable cities and communities. [15]

Figure 50: SDG 14, underwater life. [15]

Figure 51: SDG 15, life of terrestrial ecosystems. [15]

Appendix B- Plant work point

The designs of the pipes, exchangers and turbomachines have been made through their sizing under the limit conditions in which they will work. These conditions are included in the following tables:

Table 8: Working conditions of the gas cycle.

Gas Cycle					
Points	p(bar)	T(oC)	density(kg/m^3)	visco(m^2/s)	m_dot(kg/s)
1	1	15	1,21	1,484E-05	195,10
2	6,752	257	4,427	6,390E-06	195,10
3	6,752	1500	1,325	4.745E-05	201,50
4	1	940,1	0,2848	1.732E-04	201,50
5	1	540	0,4281	8,827E-05	201,50
5p	1	540	0,4281	8,827E-05	201,50
5m	1	540	0,4281	8,827E-05	201,50
6	1	335,7	0,5684	5,493E-05	201,50
7	6,752	705,7	4,373	6,524E-06	201,50
8	1	106,6	0,8998	2,502E-05	201,50

Table 9: Working conditions of the S-CO_2 cycle.

S-CO_2 cycle					
Points	p(bar)	T(oC)	density(kg/m^3)	visco(m^2/s)	m_dot(kg/s)
1	85	35	612,1	7,496E-08	443,90
2	300	72,55	777,2	8.783E-08	93,26
2_alpha	300	72,55	777,2	8.783E-08	350,64
3	299,6	400	229,8	1,543E-07	93,26
4	299,6	447,1	211,8	1.722E-07	350,64
5	299,6	437,2	215,3	1,684E-07	443,90
6	299,2	674	156,4	2,692E-07	443,90
7	86,6	510,4	57,97	6.041E-07	443,90
8	86,2	700	46,07	8,858E-07	443,90
9	85,8	452,2	62,38	5.305E-07	443,90
10	299,2	682,1	155	2,729E-07	443,90
11	299,2	674,1	156,4	2,692E-07	443,90
12	86,2	700	46,07	8,858E-07	443,90
13	85,8	443,3	63,2	5,190E-07	443,90
14	85,8	452,1	62,38	5.305E-07	443,90
15	85,4	77,55	179,1	1.143E-07	443,90
L1	85,8	78,28	179,3	1.144E-07	120,70
L2	85,4	405	66,8	4,714E-07	120,70
L3	85	77,55	177,9	1.148E-07	120,70

Table 10: Working conditions of the ORC cycle.

ORC Cycle					
Points	p(bar)	T(oC)	density(kg/m^3)	visco(m^2/s)	m_dot(kg/s)
1	50	198,9	117,5	1,423E-07	106,70
2	3,29	108,4	6,452	1.465E-06	106,70
3	3,29	49,1	7,726	1.066E-06	106,70
4	3,29	35	8,128	9,780E-07	106,70
5	50	39,43	541,9	2,585E-07	106,70
6	50	83,97	489,3	1.935E-07	106,70

References

1. E. W. Lemmon and R. T. Jacobsen, "Viscosity and thermal conductivity equations for nitrogen oxygen argon and air.", from *the International Journal of Thermophysics. Vol. 25*, January 2004, pp. 21-69.
2. R. Span y W. Wagner, «A New Equation of State for Carbon Dioxide Covering the Fluid Region from the Triple-Point Temperature to 1100 K at Pressures up to 800 MPa,» de *J. Phys. Chem, Vol. 25, No. 6*, 1996. Author 1, A.B.; Author 2, C. Title of Unpublished Work. *Abbreviated Journal Name* stage of publication (under review; accepted; in press).
3. Vesovic, «The Transport Porperties of Carbon Dioxide,» de *J. Phys. Chem, Vol.19, No. 3*, 1990.
4. A. Fenghour, W. A. Wakeham y V. Vesovic, «The Viscosity of Carbon Dioxide,» de *J. Phys. Chem, Vol. 27, No. 1*, 1998
5. H. Miyamoto y K. Watanabe, «A thermodynamic property model for fluid-phase n-butane,» de *Int. J. Thermophys.*, 2001.
6. R. A. Perkins, M. L. V. Ramires, C. A. N. d. Castro y L. Cusco, Measurement and correlation of the thermal conductivity of butante from 135 K to 600 K at pressures to 70 Mpa, J. Chem. Eng. Data 47, 2002.
7. B. A. Younglove y J. F. Ely, Thermophysical Properties of Fluids. II Methane, Ethane, Propane, Isobutane and Normal Butane., J. Phys. Chem. Ref. Data Vol. 16, No. 4, 1987.
8. G. Nellis y S. Klein, Heat transfer, Madison: University of Wisconsin, 2012
9. G. D. Dragutinovic y B. S. Baclic, Operation of Counterflow Regenerators, Billerica: Computational Mechanics Publications, 1998
10. I. P. Serrano, A. Cantizano, J. I. Linares y B. Y. Moratilla, «Modelling and sizing of the heat exchangers of a new supercritical CO2 Brayton power cycle for energy conversion for fusion reactors.,» de *Fusion Engineering and Design 89*, 2014, pp. 1905-1908
11. O. E. Baljè, Turbomachines: A Guide to Design, Selection and Theory, Wiley And Sons, 1981
12. Turbomachinery Selection, Chapter 2.
13. «Acero Inoxidable,» Bandmeyer Steel Company, [En línea]. Available: https://www.sandmeyersteel.com/spanish/310-310S.html. [Último acceso: 20 06 2022]
14. Pipe Schedules ASME/ANSI B36.10 M.
15. «Objetivos de Desarrollo Sostenible,» Naciones Unidas, [En línea]. Available: https://www.un.org/sustainabledevelopment/es/objetivos-de-desarrollo-sostenible/. [Último acceso: 04 06 2022].
16. J. I. Linares, E. Arenas, A. Cantizano, M. J. Montes, A. J. Rovira y J. Porras, «Hybrid Brayton Supercritical CO2 power cycle using a gas turbine and a tower receptor with an ORC as a waste heat recovery system,» *Proceedings of III International Conference on Engineering Thermodynamics (12 CNIT), Universidad Carlos III de Madrid,* June 29 - July 1, Madrid (Spain)
17. «Tecnología Rank – Como funciona un ORC,» Rank, 21 06 2019. [En línea]. Available: https://www.rank-orc.com/es/2019/06/21/tecnologia-rank-como-funciona-un-orc/. [Último acceso: 04 06 2022]
18. Norsok Standard, Process Design, Norway: The Norwegian Oil Industry Association (OLF) and The Federation of Norwegian Industry., 2006.
19. V. Dostal, A supercritical carbon dioxide cycle for next generation nuclear reactors, Doctoral Thesis, Massachusetts Institute of Technology, 2004.
20. F. Noguera y E. A. José Ignacio Linares, Sistema de conversión de potencia para central termosolar de torre basado en ciclo de Brayton con CO2 supercrítico, Madrid: Universidad Pontificia de Comillas, 2020